JETP LETTERS VOLUME 69, NUMBER 5 10 MARCH 1999

On the possible enhancement of the magnetic field by neutrino reemission processes in the mantle of a supernova

A. A. Gvozdev* and I. S. Ognev
P. G. Demidov Yaroslavl State University, 150000 Yaroslavl, Russia

(Submitted 19 October 1998; resubmitted 8 February 1999)
Pis'ma Zh. Éksp. Teor. Fiz. **69**, No. 5, 337–342 (10 March 1999)

Urca neutrino reemission processes under the conditions in the mantle of a supernova with a strong toroidal magnetic field are investigated. It is shown that P-parity violation in these processes can be manifested macroscopically as a torque that rapidly spins up the region of the mantle occupied by such a field. Neutrino spin-up of the mantle can strongly affect the mechanism of further generation of the toroidal field, specifically, it can enhance the field in a small neighborhood of the rigid-body-rotating core of the progenitor star. © *1999 American Institute of Physics.* [S0021-3640(99)00105-X]

PACS numbers: 97.60.Bw, 95.30.Cq

The problem of the shedding of the mantle in an explosion of a type-II supernova is still far from a complete solution.[1] It is known that in several seconds after the collapse of a presupernova an anomalously high neutrino flux with typical luminosities $L\sim10^{52}$ ergs/s is emitted from the neutrinosphere, which is approximately of the same size as the remnant of the collapse (core).[2] In principle, such a neutrino flux could initiate a process leading to the shedding of the mantle as a result of the absorption and scattering of neutrinos neutrinos by nucleons and the e^+e^- plasma of the medium.[3] However, detailed calculations in spherically symmetric collapse models have shown that such processes are too weak for mantle shedding.[4] In a magnetorotational model,[5] mantle shedding is initiated by the outward pressure of a strong toroidal magnetic field generated by the differential rotation of the mantle with the core's primary poloidal magnetic field frozen into it. Indeed, as calculations show,[6] a toroidal field $B_0\sim10^{15}$–10^{16} G is generated in ~1 s during millisecond periods rotation in a poloidal field $B\sim10^{12}$–10^{13} G. We note that the model of Ref. 5 contains a fundamental limit on the energy of the toroidal field (it cannot exceed the kinetic energy of the ''core + shell'' system) and therefore on the maximum field itself.

In the present letter we investigate the possibility that this magnetic field ''frozen in'' the mantle is enhanced as result of elementary neutrino reemission processes occurring in the mantle. We assume the mantle in the vicinity of the neutrinosphere to be a hot ($T\sim$ several MeV) and quite dense (though transparent to neutrinos, $\rho\sim10^{11}$–10^{12} g/cm^3) medium consisting of free nucleons and e^+e^- plasma. Under these conditions the dominant neutrino reemission processes are the Urca processes:

$$p + e^- \rightarrow n + \nu_e , \tag{1}$$

$$n + e^+ \rightarrow p + \tilde{\nu}_e , \tag{2}$$

$$n + \nu_e \rightarrow p + e^- , \tag{3}$$

$$p + \tilde{\nu}_e \rightarrow n + e^+ \tag{4}$$

(we note that β decay is statistically suppressed in such a medium). The basic idea of this letter is as follows. In an external magnetic field, neutrinos are emitted and absorbed asymmetrically with respect to the direction of the magnetic field as a result of P-parity violation in the processes (1)–(4).[7] Therefore a macroscopic torque spinning up the mantle can arise in a toroidal field. It is known[8] that for an equilibrium neutrino distribution function such a neutrino-recoil momentum must be zero. However, the supernova region under consideration is nonequilibrium for neutrinos, so that the torque that arises in it is different from zero. Moreover, as we shall show below, the torque can be large enough to change substantially the distribution of the angular rotational velocities of the mantle in the region filled with a strong magnetic field over the characteristic neutrino-emission times. According to the equation governing the generation of a toroidal field,[6] a large change in the gradient of the angular velocities in this region can lead to redistribution of the magnetic field (specifically, enhancement of the field in a small neighborhood of the rigid-body-rotating core).

A quantitative estimate of the effect follows from the expression for the energy–momentum transferred by neutrinos to a unit volume of the mantle per unit time

$$\frac{dP_\alpha}{dt} = \frac{1}{V} \int \prod_i dn_i f_i \prod_f dn_f (1 - f_f) \frac{|S_{if}|^2}{\mathscr{T}} k_\alpha , \tag{5}$$

where dn_i and dn_f are, respectively, the number of initial and final states in an element of the phase volume, f_i and f_f are, respectively, the distribution functions of the initial and final particles, k_α is the neutrino momentum, and $|S_{if}|^2/\mathscr{T}$ is the squared S-matrix element per unit time. It is of interest to calculate the latter under our conditions, since, as far as we know, the Urca processes (1)–(4) have been previously studied for relatively weak[9] ($B \lesssim m_e^2/e$) and very strong[10] ($B \sim m_p^2/e$) fields. Assuming that the e^+e^- plasma mainly occupies only the lowest Landau level ($\mu_e \lesssim \sqrt{2eB}$, where μ_e is the chemical potential of the electrons), we obtained the following expression for the squared S-matrix element summed over all proton Landau levels and the polarizations of the final particles and averaged over the polarizations of the initial particles:

$$\begin{aligned} |S_{if}|^2 = {} & \frac{G_F^2 \cos^2\theta_c (2\pi)^3 \mathscr{T}}{2 L_y L_z V^2} \cdot \frac{\exp(-Q_\perp^2/2eB)}{4\omega\varepsilon} \\ & \times \frac{1}{2} \left[\sum_{n=0}^{\infty} \frac{|M_+|^2}{n!} \left(\frac{Q_\perp^2}{2eB} \right)^n \cdot \delta^{(3)} + \sum_{n=1}^{\infty} \frac{|M_-|^2}{(n-1)!} \left(\frac{Q_\perp^2}{2eB} \right)^{n-1} \cdot \delta^{(3)} \right], \end{aligned} \tag{6}$$

$$\begin{aligned} |M_\sigma|^2 = {} & 4(1 + g_a\sigma)^2 [2(up)(uk) - (pk) - (up)(k\tilde{\varphi}u) - (uk)(p\tilde{\varphi}u)] \\ & + 8 g_a^2 (1 + \sigma)[(pk) - (p\tilde{\varphi}k)], \end{aligned} \tag{7}$$

where $u_\alpha=(1,0,0,0)$, $\mathbf{B}=(0,0,B)$, and $\delta^{(3)}$ is a delta function of the energy, momentum in the direction of the magnetic field, and one transverse component of the momentum, which are conserved in the reactions; $(pk)=\varepsilon\omega-p_3k_3$, $p^\alpha=(\varepsilon,\mathbf{p})$ and $k^\alpha=(\omega,\mathbf{k})$ are the 4-momenta of the electron and neutrino, $Q_\perp^2$ is the square of the momentum transfer transverse to the magnetic field in the reactions (1) and (3) [with the corresponding substitutions $p\to-p$ and $k\to-k$ in the crossing reactions (2) and (4)], $\tilde{\varphi}_{\alpha\beta}=\tilde{F}_{\alpha\beta}/B$ is the dimensionless dual magnetic-field tensor, $\sigma=\pm1$ is the projection of the proton spin on the direction of the magnetic field, n is the summation index over the proton Landau levels, $\mathscr{T}V=\mathscr{T}L_xL_yL_z$ is the normalization four-volume, g_a is the axial constant of the nucleonic current, G_F is the Fermi constant, and θ_c is the Cabibbo angle. We note that in the limit of a strong magnetic field, when the protons occupy only the ground Landau level, expressions (6) and (7) agree with the result obtained previously in Ref. 10.

Analysis shows Urca processes are the fastest reactions in our medium, and they transfer the medium into a state of β equilibrium in $\sim10^{-2}$ s. Therefore we employed the condition of β equilibrium and singled out in the expression for the energy–momentum transfer to the shell (5) the separate contributions from processes involving neutrinos (1), (3) and antineutrinos (2), (4):

$$\frac{dP_\alpha^{(\nu,\tilde{\nu})}}{dt}=\int\frac{d^3k}{(2\pi)^3}k_\alpha\left(1+\exp\left(\frac{-\omega+\mu_{(\nu,\tilde{\nu})}}{T}\right)\right)\mathscr{K}^{(\nu,\tilde{\nu})}\delta f^{(\nu,\tilde{\nu})}. \tag{8}$$

Here $\delta f^{(\nu,\tilde{\nu})}$ is the deviation of the distribution function from the equilibrium function, $\mathscr{K}^{(\nu,\tilde{\nu})}$ is the (anti) neutrino absorption coefficient, defined as

$$\mathscr{K}^{(\nu,\tilde{\nu})}=\frac{1}{V}\int\prod_i dn_if_i\prod_f dn_f(1-f_f)\frac{|S_{if}|^2}{\mathscr{T}}, \tag{9}$$

where the integration extends over all states except the neutrino states in the reaction (3) and antineutrino states in the reaction (4), respectively. As follows from Eq. (8), actually, the momentum transferred to the medium is different from zero only if the neutrino distribution function deviates from the equilibrium distribution.

To calculate the absorption coefficient $\mathscr{K}^{(\nu,\tilde{\nu})}$ we assumed that the ultrarelativistic e^+e^- plasma occupies only the ground Landau level, while the protons occupy quite many levels (the dimensionless parameter $\delta=eB/m_pT$ is much less than one). We also used the fact that at the densities under consideration the nucleonic gas is Boltzmannian and nonrelativistic. Then, dropping terms $\sim\delta$, we can write expression (9) in the form

$$\begin{aligned}\mathscr{K}^{(\nu,\tilde{\nu})}=&\frac{G_F^2\cos^2\theta_c\,eB\,N_{(n,p)}}{2\pi}((1+3g_a^2)-k_3/\omega\cdot(g_a^2-1))\\&\times\left(1+\exp\left(\frac{\pm(\mu_e-\triangle)-\omega}{T}\right)\right)^{-1},\end{aligned} \tag{10}$$

where N_n, N_p, m_n, and m_p are, respectively, the densities and masses of the neutrinos and protons, $\Delta=m_n-m_p$, and ω and k_3 are, respectively, the neutrino energy and the neutrino momentum in the direction of the magnetic field.

For further calculations we employed the neutrino distribution function in the model of a spherically symmetric collapse of a supernova in the absence of a magnetic field.[11]

This is a quite good approximation when the region occupied by the strong magnetic field is smaller than or of the order of the neutrino mean-free path. By strong we mean a field in which the e^+e^- plasma occupies only the ground Landau level: $eB \gtrsim \mu_e^2$. In the model of Ref. 6 the region occupied by such a field is no greater than several kilometers in size, and we estimate the neutrino mean-free path in this region as

$$l_\nu \simeq 4 \ \text{km} \cdot (B/4.4\times 10^{16}\,\text{G})^{-1} (\rho/5\times 10^{11}\,\text{g/cm}^3)^{-1}. \tag{11}$$

Therefore the magnetic field cannot strongly alter the neutrino distribution function, and our approximation is quite correct.

As calculations of the components of the energy–momentum (8) transferred to the medium during neutrino reemission showed, the radial force arising is much weaker than the gravitational force and cannot greatly influence the mantle dynamics. However, the force acting in the direction of the magnetic field can change quite rapidly the distribution of the angular velocities in the region occupied by the strong magnetic field. The density of this force can be represented as

$$\mathfrak{J}_\parallel^{(\text{tot})} = \mathfrak{J}_\parallel^{(\nu)} + \mathfrak{J}_\parallel^{(\tilde{\nu})} = \mathcal{N}\left[(3\langle\mu^2\rangle_\nu - 1) I(a) e^{-a} + (3\langle\mu^2\rangle_{\tilde{\nu}} - 1) I(-a)\right], \tag{12}$$

$$\langle\mu^2\rangle = \left(\int \mu^2\, \omega\, f\, d^3k\right)\left(\int \omega\, f\, d^3k\right)^{-1},$$

where μ is the cosine of the angle between the neutrino momentum and the radial direction, and

$$I(a) = \int_0^\infty y^3 (e^{y-a}+1)^{-1} dy, \quad a = \mu_e/T.$$

In deriving Eq. (12) we made the standard assumption that the local distribution function factorizes in a medium that is sufficiently transparent to neutrinos: $f^{(\nu,\tilde{\nu})} = \phi^{(\nu,\tilde{\nu})}(\omega/T_\nu)\Phi^{(\nu,\tilde{\nu})}(r,\mu)$, where T_ν is the neutrino spectral temperature.[1] To estimate the force in the diffusion region we assumed that $T_\nu \simeq T$ and chose $\phi^{(\nu,\tilde{\nu})}(\omega/T_\nu) = \exp(-\omega/T_\nu)$. We determined the dimensional parameter $\mathcal{N}$ in expression (12) as

$$\mathcal{N} = \frac{G_F^2 \cos^2\theta_c}{(2\pi)^3}\,\frac{g_a^2 - 1}{3}\, eBT^4 N_N$$

$$\simeq 4.5\times 10^{20} (\text{dynes/cm}^3) \left(\frac{T}{5\ \text{MeV}}\right)^4 \left(\frac{B}{4.4\times 10^{16}\,\text{G}}\right) \left(\frac{\rho}{5\times 10^{11}\,\text{g/cm}^3}\right), \tag{13}$$

where $N_N = N_n + N_p$ is the total nucleon density.

The force (12) was estimated numerically in the diffusion region of the supernova atmosphere for typical (excluding the field) values of the macroscopic parameters for this region: $T = 5$ MeV, $B = 4.4\times 10^{16}$ G, $\rho = 5\times 10^{11}$ g/cm^3. For these values $a \simeq 3$, $\langle\mu^2\rangle_\nu \simeq \langle\mu^2\rangle_{\tilde{\nu}} \simeq 0.4$ (Ref. 11), and the density of the forces in the direction of the field can be estimated from Eq. (12) as

$$\mathfrak{J}_\parallel^{(\text{tot})} \simeq \mathfrak{J}_\parallel^{(\nu)} \simeq \mathcal{N}. \tag{14}$$

We note that the angular acceleration produced by the torque exerted by such a force is large enough to spin up the region of the mantle containing a strong magnetic field to typical velocities of fast pulsars ($P_0 \sim 10^{-2}$ s) in a characteristic time ~ 1 s. In our opinion, this result is of interest in itself and can serve as a basis for a number of applications. However, we shall give a qualitative discussion of only one possible manifestation of this result — the effect of such a fast spin-up of the mantle on the further generation of the toroidal magnetic field. Indeed, if the modification of the gradient of the angular velocities of the mantle is large, the toroidal magnetic field in the mantle at subsequent times will vary according to a law that is different from the linear law.[6] Analysis of the equation governing the generation of a toroidal field with allowance for the force (14), which is linear in this field, leads to the conclusion that its growth in time is much faster (exponential) in the quite small region in which the force acts ($eB \gtrsim \mu_e^2$). However, the main source of energy of the magnetic field, just as in the case when there is no force, is the kinetic energy of the rigid-body-rotating core. Thus the force (14) can lead to a peculiar rearrangement of the region occupied by the strong field: Specifically, with virtually no change in energy, the magnetic field can become concentrated in a narrower spatial region and can therefore have in that region higher intensities, on average, than in the absence of the spin-up force. We note that the effect under discussion can strongly influence the mantle-shedding process and also the mechanism leading to the formation of an anisotropic γ-ray burst in the explosion of a supernova with a rapidly rotating core.[12] However, in order to perform detailed calculations of the generation of a toroidal field, the enhancement of the field on account of the ''neutrino spin-up,'' and the effect of this enhancement on the indicated processes, it is necessary to analyze the complete system of MHD equations, which lies far outside the scope of the present work and is a subject of a separate investigation. Qualitative estimates show that magnetic fields $B \sim 10^{17}$ G can be generated by the above-described mechanism in a small neighborhood ~ 1 km of a rapidly rotating core ($P_0 \sim 5 \times 10^{-2}$ s), and this region decreases with increasing period.

In summary, we have shown that Urca neutrino reemission processes can produce, in the region of the mantle that is filled with a strong toroidal magnetic field, angular accelerations which are sufficiently large as to greatly influence the mechanism of further generation of the field. Specifically, such rapid redistribution of the angular velocities can enhance the field in a small neighborhood of the rigid-body-rotating core of a progenitor star.

We are grateful to S. I. Blinnikov for fruitful discussions and for assistance in formulating the problem and to N. V. Mikheev and M. V. Chistyakov for helpful discussions. This work was partially supported by INTAS (Grant No. 96-0659) and the Russian Fund for Fundamental Research (Grant No. 98-02-16694).

*e-mail: gvozdev@univ.uniyar.ac.ru

[1] G. G. Raffelt, *Stars as Laboratories for Fundamental Physics*, University of Chicago Press, Chicago, Ill., 1996.

[2] V. S. Imshennik and D. K. Nadezhin, *Supernova 1987A in the Large Magellanic Cloud: Observations and Theory* [Vol. VII of Soviet Scientific Reviews (1988–1989), Series E (Astrophyics and Space Physics)], Harwood Academic Publishers, Chur, Switzerland.

[3] S. A. Colgate and R. H. White, Astrophys. J. **143**, 626 (1966).

[4] D. K. Nadyozhin, Astrophys. Space Sci. **49**, 399 (1977); **51**, 283 (1977); **53**, 131 (1978).
[5] G. S. Bisnovatyĭ-Kogan, *Physical Problems of the Theory of Stellar Evolution* [in Russian], Nauka, Moscow, 1989.
[6] G. S. Bisnovatyi-Kogan and S. G. Moiseenko, Astron. Astrophys. Trans. **3**, 287 (1993).
[7] N. N. Chugaĭ, Pis'ma Astron. Zh. **10**, 210 (1984) [Sov. Astron. Lett. **10**, 87 (1984)].
[8] D. Lai and Y.-Z. Qian, Astrophys. J. **495**, L103 (1998).
[9] O. F. Dorofeev *et al.*, JETP Lett. **40**, 917 (1984).
[10] L. B. Leinson and A. Perez, http://xxx.lanl.gov/abs/astro-ph/9711216.
[11] S. Yamada, H.-T. Janka, and H. Suzuki, http://xxx.lanl.gov/abs/astro-ph/9809009.
[12] A. MacFadyen and S. E. Woosley, http://xxx.lanl.gov/abs/astro-ph/9810274.

Translated by M. E. Alferieff

JETP LETTERS VOLUME 69, NUMBER 5 10 MARCH 1999

Excitation of tantalum-181 nuclei in a high-temperature femtosecond laser plasma

A. V. Andreev, R. V. Volkov, V. M. Gordienko, P. M. Mikheev,
A. B. Savel'ev,* E. V. Tkalya, O. V. Chutko, and A. A. Shashkov
International Laser Center, Department of Physics, and Scientific-Research Institute of Nuclear Physics, M. V. Lomonosov Moscow State University, 119899 Moscow, Russia

A. M. Dykhne
Troitsk Institute of Innovational and Thermonuclear Studies, 142092 Troitsk, Moscow Region, Russia

(Submitted 25 January 1999)
Pis'ma Zh. Éksp. Teor. Fiz. **69**, No. 5, 343–348 (10 March 1999)

The excitation of nuclei in a laser plasma is observed. Gamma rays from the radiative decay of the isomeric level $9/2^-$ (6.238 keV) ^{181}Ta in a high-temperature femtosecond Ta laser plasma are detected. © *1999 American Institute of Physics.* [S0021-3640(99)00205-4]

PACS numbers: 52.20.Jm, 52.25.Nr, 23.20.Lv, 27.70.+q

1. The possibility of observing the excitation of low-lying nuclear levels in a plasma produced by irradiating a solid-state target with an intense laser pulse has been under discussion now for more than 20 years.[1–8] Both the nuclear excitation process itself and the diagnostics and spectroscopy not only of the low-lying nuclear levels but also of the plasma are of interest. The main mechanisms responsible for the excitation of such levels (with energy less than 20 keV) in a laser plasma are considered to be photoexcitation by the characteristic x rays of the plasma,[2] inelastic scattering of the plasma electrons,[5] inverse internal conversion,[1] and some others.[5,6] Few experimental attempts have been made to observe the excitation of nuclei in plasmas,[3,4] and these attempts were unsuccessful.[5] The difficulties are due to the fact that the efficiency of the excitation process using nanosecond laser pulses is low because of the low electron temperature and low density of the plasma.

In the present letter we report the experimental observation of the excitation of nuclei in a dense high-temperature plasma produced by a femtosecond pulse for the low-lying isomeric level $9/2^-$ (6.238 keV) ^{181}Ta.

2. The possibility of efficient excitation using an ultraintense subpicosecond laser pulse with an on-target intensity of the order of 10^{16} W/cm^2 was first pointed out in Ref. 7 for the excitation of the 1.561 keV level of the isotope ^{201}Hg. Further analysis showed that the excited level of ^{201}Hg decays by electronic internal conversion followed by deexcitation in the electronic subsystem via Koster–Kronig and Auger processes. Thus the effect can be detected experimentally only from the emergence of electrons and UV radiation.

A simpler approach uses stable isotopes with a first level lying above 5 keV, which

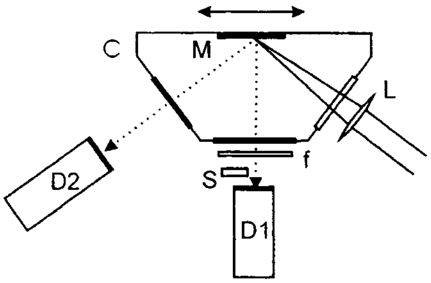

FIG. 1. Experimental arrangement (*C* is the vacuum chamber).

possess smaller electronic internal conversion coefficients, so that there is a high probability that the nuclear excitation will decay via emission of a γ ray.[8] The fact that the typical lifetimes of such isomeric levels are longer than the x-ray emission time of the plasma (the latter does not exceed 2–3 ps in the region of photon energies above 5 keV) makes it possible to detect γ rays using time-resolved methods.

We chose as the object of investigation the stable isotope ^{181}Ta. We proceeded from the following considerations: 1) 100% isotope content in the natural sample; 2) relatively high energy of the first excited level 6.238 keV; 3) the lifetime ~ 6 μs, making it possible to implement easily the time-resolved method using a standard NaI(Tl) scintillation detector; and, 4) the possibility of performing comparative experiments with a W sample (the natural mixture of the stable isotopes of W makes it possible to obtain a plasma whose characteristics are virtually identical to a Ta plasma).

Preliminary estimates of the efficiency of different channels of excitation of the $9/2^-$ (6.238 keV) level of the isotope ^{181}Ta are presented in Ref. 8. Specifically, excitation due to the hot electronic component with electron temperature 3–10 keV, which is achieved in a femtosecond plasma with laser radiation intensities 10^{16}–10^{17} W/cm^2, was studied. The nonstationary nature of the plasma and the Doppler broadening of the nuclear level are taken into account systematically. These estimates show that the effect can be realistically detected in the single γ-ray counting mode.

3. The experimental arrangement is displayed in Fig. 1. The radiation from a femtosecond dye laser (wavelength 600 nm, pulse duration 200 fs) was focused on the target *M* by an objective lens *L*, which gave an intensity of $(1–5)\times 10^{16}$ W/cm^2 with *F*/6 focusing. The x rays and γ rays from the plasma were detected through the exit windows (100 μm thick beryllium foils) of the cell using two NaI(Tl) scintillation x-ray detectors *D*1 and *D*2 with an FÉU-119 photomultiplier. The signal from the *D*2 detector was fed into a charge-sensitive amplifier and detected using an analog-to-digital converter (ADC), yielding in each laser shot information about the total yield of x radiation from the plasma in the region $E > 3$ keV. The signal from the detector *D*1 either entered along a similar channel into a different ADC input (in this case the detector was also equipped with additional x-ray filters *f*) or was detected, through a 50 Ω load, by a digital oscillograph with 10 ns time resolution. The total time resolution of such a channel was determined by the characteristic emission time of a NaI(Tl) scintillator, equal to 255 ns.[9] This detector provided a detection solid angle of 0.07 sr (the target-to-*D*1 distance was about 5 cm).

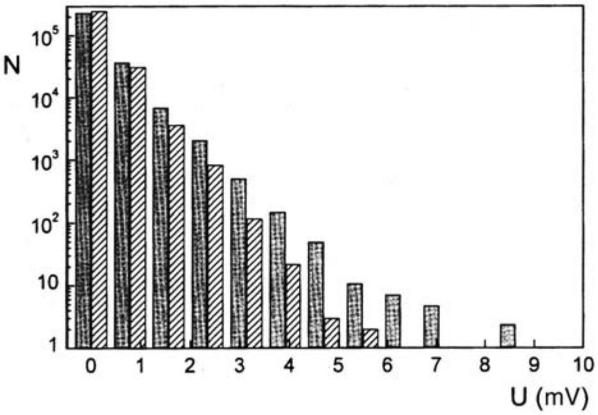

FIG. 2. Distribution of the number N of counts versus the pulse height U. Light columns — W target with an Fe-55 source, dark columns — no source.

The radioactive source S (^{55}Fe sample, emitting 5.9 keV Mn $K_{\alpha1,2}$ x rays) served for calibrating the $D1,2$ detectors. Assuming the signal at the output of the scintillation detector to be a linear function of the x-ray energy, we determined for a 6.238 keV gamma ray the average amplitude of the output signal to be 2.0 meV with HWHM of 0.8 mV.

4. The basic features of the typical experimental implementation in the time-resolved mode, which are characteristic for both types of targets, are as follows: (i) a ~ 5 V pulse, determined by the plasma x rays and decaying to a level below 5 mV with a delay of $t \sim 3$ μs relative to the time of plasma ignition; (ii) a ~ 2 mV ''noise'' component with $t \sim 3$ μs, greatly exceeding the intrinsic noise of the detector (<0.2 mV) and decaying gradually with characteristic time ~ 100 μs. The presence of a large-amplitude pulse prevents analysis for delay times $t < 3$ μs, which were excluded from the analysis. The noise signal is due to the slow afterglow components of the scintillator.[9]

To estimate the probability of detecting a gamma ray against the background of the noise signal, a control experiment was performed with a W target. In this experiment, besides x rays from the plasma, x rays from the source S were incident on the detector $D1$. The amplitude distribution of the pulses obtained from 100 time series is displayed in Fig. 2. On the basis of the activity of the source S, we were able to detect 1350 x-ray photons, but a substantial fraction of these photons give pulses with amplitude less than 1 mV and are not detected against the noise background. The excess number of ''events'' (pulses with amplitude greater than 3 mV) in the presence of the source S is about 700. Thus the probability of detecting a 5.9 keV x-ray photon as an event exceeds 50% in our experiments. The corresponding probability should be higher for 6.238 keV gamma rays.

5. The experiment was performed with two targets — Ta and W. In addition, some time series were obtained with an additional filter *f*, consisting of a 300 μm aluminum foil (Ta + f), on the detector $D2$. Such a filter attenuates the 6-keV radiation by a factor of 1000 with the total signal at the detector decreasing by approximately a factor of 3. For this reason, the time series obtained in this case should not contain gamma rays from an

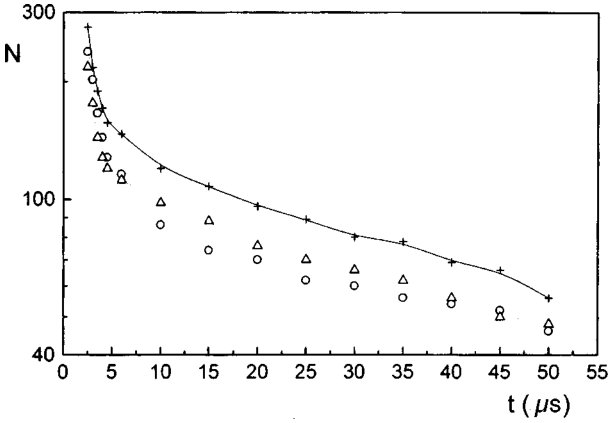

FIG. 3. Total number of N events in the time-delay interval from t to 100 μs as a function of t: + — Ta target, Δ — W target, ○ — Ta + f target.

isomeric transition from the level $9/2^-$ (6.238 keV) into the ground state of the ^{181}Ta nucleus.

To equalize the noise level for the Ta and W targets, only the time series corresponding to a fixed range of values of the total yield of x rays measured with the $D2$ detector were analyzed, and for the Ta + f target time series with a total yield three times higher than the total yield on the Ta and W targets were chosen. Time series with total yields less than the lower limit of that range corresponded to laser intensities less than 10^{16} W/cm^2 and, as a rule, contained no events. The average noise level for time series with total yields above the upper limit of that range (intensity above 4×10^{16} W/cm^2) exceeded 3 mV, which made analysis impossible. Thus we found the optimal experimental parameters (laser intensity, geometry, detector characteristics) for detecting single gamma rays.

A total of 100 time series for each type of target were analyzed. Analysis of the results displayed in Fig. 3 shows that in the entire range from 3 to 100 μs a reliable excess of events is observed for the Ta target above the analogous value for W. The introduction of a filter decreases the number of events on the Ta target to levels characteristic for the W target. In the entire time interval from 3 to 100 μs the total number of events on the Ta target was greater by 49 than the number of events on the W target. Therefore, on the average, in every-other time series we observe a gamma ray due to the decay of the isomeric level $9/2^-$ (6.238 keV) ^{181}Ta. Taking account of the detection solid angle of the detector $D1$ and the 50% probability of observing a gamma ray using our method, the total number of radiative decays per time series is $\sim$200. It should be noted that the total number of excited nuclei in the plasma, when one takes into account the conversion channel of decay (the internal conversion coefficient of this level in a neutral atom is 70.5) and the limited interval of time delays ($t>3$ μs), should be much higher.

6. An important feature of the data obtained (see Fig. 3) is the observation of gamma decays of nuclei in times a factor of 10 longer than the total lifetime of the excited level of ^{181}Ta in a neutral atom (6.04 μs). This could be due to the decrease of the electronic

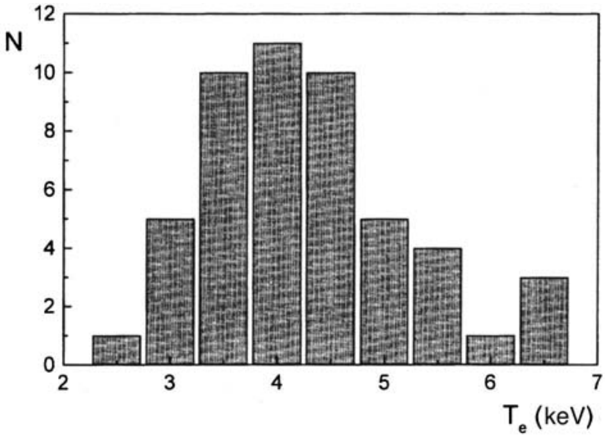

FIG. 4. Histogram of the distribution of the hot-electron temperature T_e for 50 laser shots.

internal conversion probability as a result of ionization of all upper atomic shells right up to the M shell inclusive (the time corresponding to radiative width of the excited level $9/2^-$ (6.238 keV) ^{181}Ta is ~430 μs). Estimates obtained by solving the equations governing the nonstationary ionization kinetics[10] show that for electron temperatures ~1 keV and solid-state ion densities the degree of plasma ionization reaches $Z\sim 60$ in 1 ps (we recall that the Ta nuclear charge is 73). Thus, for some excited Ta nuclei there may be not be any electrons in any electronic shells all the way up to $3S_{1/2}$. Electronic recombination of such nuclei, which have escaped from the plasma volume as a result of hydrodynamic expansion, will be slow because of the low electron density and will occur partially at the walls of the cell. The transit time of Ta ions up to the wall is estimated to be 1–100 μs, based on the velocity of hydrodynamic expansion of the plasma. All this indicates that diagnostics of the degree of ionization of a hot dense plasma according to the shape of the decay curve of the excited nuclei is possible in principle.

The experiments and estimates presented in Ref. 8 show that most of the intrinsic plasma x rays with energies above 3 keV are due to the hot electronic component. Therefore, to estimate the probability of photoexcitation of a ~6 keV nuclear level in a plasma it is necessary to have data on the temperature of hot electrons. For this purpose an additional experiment was performed. In this experiment both detectors measured simultaneously the total yield of hard x rays from the Ta plasma. X-ray notch filters were placed in front of the entrance window of the $D1$ detector (see Ref. 8 for a more detailed discussion). The results are presented in Fig. 4. The average temperature of the hot electrons was 4 ± 1 keV, which, according to our estimates, should lead to photoexcitation of approximately 10^2–10^3 nuclei over each laser flash in a 0.1 μm thick and 5 μm in diameter plasma layer. It should be noted that the actual volume where nuclei are excited is much larger than the plasma layer. Indeed, the depth of the crater on the target surface (corresponding to the heated layer) is ~1 μm. In addition, the mean-free path of 6-keV x rays in metallic Ta is about 2 μm. Therefore it is very likely that a definite number of nuclei can be excited in the unvaporized part of the tantalum target.

Our estimates are consistent with the experimental results. However, to obtain a more complete description of the nuclear excitation processes in a plasma it is necessary to take systematically into account such factors as the real kinetics of a nonstationary dense, highly ionized, hot plasma, the interaction of nuclei with the magnetic fields induced in the plasma, which reach tens of megagauss, and other factors.

Our data open up new prospects in the nuclear spectroscopy of low-lying isomeric levels, for diagnostics of a hot, dense plasma according to the products and kinetics of nuclear decay, as well as for solving the problem of a population inversion on isomeric levels for producing a gamma-ray laser, and so on.

We are extremely grateful to Nikolaĭ Ivanovich Koroteev for repeated discussions that greatly stimulated the successful completion of this work.

We also thank Yu. V. Ponomarev and V. P. Petukhov for fruitful discussions concerning this work and for assistance in calibrating the apparatus.

This work was supported by Russian Fund for Fundamental Research under Grants Nos. 97-02-17013a, 98-02-16070a, and 96-02-19146a, the program ''Russian Universities,'' and Grants Nos. 96-15-96460 and 96-15-96481 in Support of the Leading Scientific Schools.

*e-mail: savelev@femto.ilc.msu.su

---

[1] V. I. Gol'danskiĭ and V. A. Namiot, JETP Lett. **23**, 451 (1976).
[2] V. S. Letokhov and E. A. Yukov, Laser Phys. **4**, 382 (1994).
[3] Y. Izawa and C. Yamanaka, Phys. Lett. B **88**, 59 (1979).
[4] R. V. Arutyunyan, L. A. Bol'shov, V. D. Vikharev *et al.*, Yad. Fiz. **53**, 36 (1991) [Sov. J. Nucl. Phys. **53**, 23 (1991)].
[5] E. V. Tkalya, JETP Lett. **53**, 463 (1991).
[6] R. V. Arytunyan, L. A. Bolshov, V. F. Strizhov, and E. V. Tkalya, Sov. Tech. Rev. B. Thermal Phys. **4**, Pt. 2, 1 (1992).
[7] A. V. Andreev, V. M. Gordienko, A. M. Dykhne *et al.*, JETP Lett. **66**, 331 (1997).
[8] A. V. Andreev, R. V. Volkov, V. M. Gordienko *et al.*, Kvant. Élektron. **26**, 55 (1999).
[9] M. N. Medvedev, *Scintillation Detectors*, Atomizdat, Moscow, 1977.
[10] R. V. Volkov, V. M. Gordienko, M. S. Dzhidzhoev *et al.*, Kvant. Élektron. (Moscow) **24**, 1114 (1997).

Translated by M. E. Alferieff

JETP LETTERS VOLUME 69, NUMBER 5 10 MARCH 1999

On the phase state of the core matter in a high-power discharge through a wire

S. A. Pikuz, G. V. Ivanenkov,* and T. A. Shelkovenko
P. N. Lebedev Physics Institute, Russian Academy of Sciences, 117924 Moscow, Russia

D. Hammer
Laboratory of Plasma Studies, 369 Upson Hall, Cornell University,
14853 Ithaca, NY, USA

(Submitted 25 January 1999)
Pis'ma Zh. Éksp. Teor. Fiz. **69**, No. 5, 349–354 (10 March 1999)

Experimental facts attesting to a two-phase (liquid-metal–vapor) state of the matter in the core produced in a high-power discharge through thin wires are presented. The modern technique of multiframe x-ray shadow photography has made it possible to observe vapor bubbles in the core and their interaction with the shock wave penetrating from the corona. © *1999 American Institute of Physics.* [S0021-3640(99)00305-9]

PACS numbers: 52.80.Qj

In high-power discharges in a diode loaded with fine wires, cores of dense and cold matter surrounded by a plasma corona have been observed along the axes.[1,2] In isolated wires the core existed independently, expanding only slowly under the inertia of the initial explosion, up until the arrival of the compression shock wave from the corona. The interaction of this shock wave with the core drove instabilities at the core–corona interface.[2] In multiwire discharges, the cores, after expanding explosively up to several initial diameters, thereafter for tens of nanoseconds either remained without any visible changes or swelled slowly in a manner preserving the similarity of the exterior contours. The degree of the axial nonuniformity of the explosion depended strongly on the wire material and diameter as well as the growth rate of the current through the load.[3,4] For cylindrical loads, in images obtained previously by laser probing[5,6] the body of the wires could be seen right up to the moment of generation of the x-ray pulse as the plasma converged on the axis.

X-ray probing showed[2,3] that the core possessed 1) a sharp boundary with a density differential of one or two orders of magnitude over a thickness <2–$5\ \mu$m, and 2) a fine interior structure with a characteristic scale of 10–50 μm. The core can be expected to be in a state of a boiling liquid metal.[1,7] Objects of this kind have been little studied, and even this conjecture itself has still not been confirmed. Our aim in the present work is to do this.

The investigations were conducted on the *XP* pulsed power generator at Cornell University (480 kA, 100 ns) using the method of direct x-ray probing of a plasma load using the radiation from an *X* pinch[1–3] (one-frame exposure time $\lesssim 1$ ns, spatial resolution

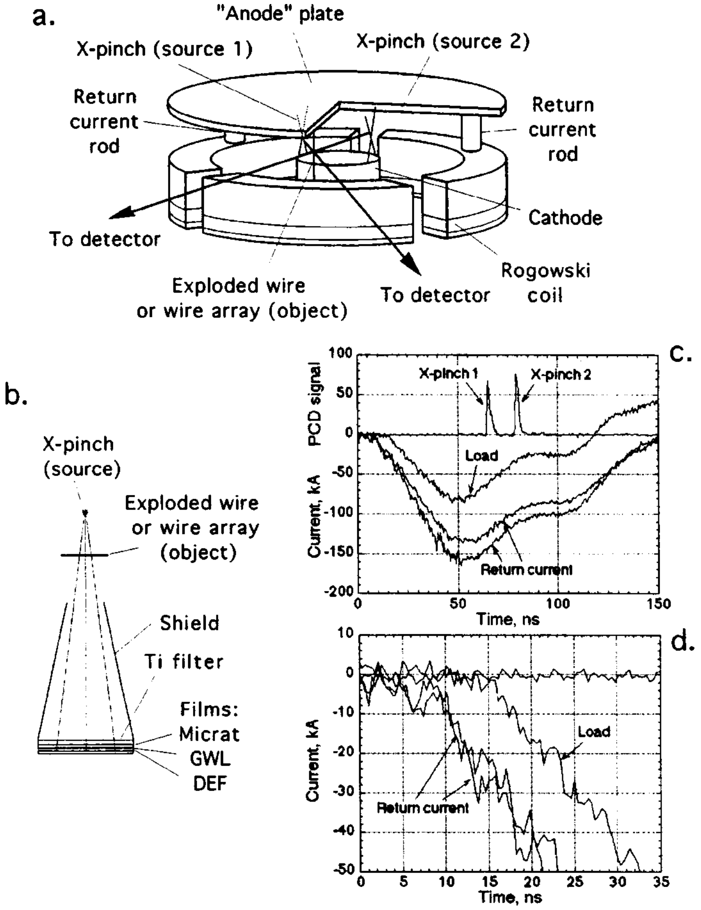

FIG. 1. Experimental arrangement, typical current pulses, and signals from the Rogowski loops.

1–3 μm, and range of detection 1–4 Å). A diagram of the experiment is shown in Fig. 1.

A series of results obtained with load currents 80–120 kA is shown in Figs. 2, 3, and 4. The first figure shows two photographs (a, b) of the explosion of a nickel wire 25 μm in diameter. These photographs were obtained in one shot. Virtually the entire core volume is filled with foam containing distinct bubbles, and splashes of liquid metal can be seen at a number of locations on the surface in the photograph taken at 51 ns. The shock front is located at first near the boundary of the core. Then it converges toward the axis, destroying the structure of the foam, and after reflecting it leaves behind an almost uniform medium. A similar picture is also observed for the explosion of a copper wire (Fig. 2e), but here the core is thicker and the surface is more open.

A similar picture also obtains for the pair tungsten–gold. In tungsten (Fig. 3a) the macroinstability (on a scale of hundreds of μm) of the core–corona boundary is more noticeable than in copper; a small-scale (several μm) structure as well as ejecta of matter which weakly absorb x rays are observed at bulges of the core. In the gold wire (Fig. 3b) this structure resembles an elastic tube with a thin (sometimes, double) wall, which at

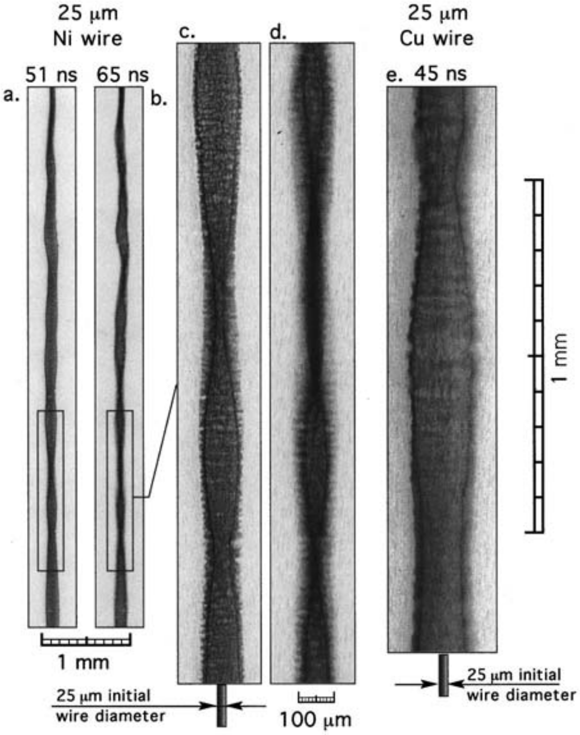

FIG. 2. Shadowgrams of discharges through Ni and Cu wires.

some locations is torn from the inside and which is filled with matter with a much lower density.

In multiwire loads there were many fewer large-scale perturbations of the core boundaries, and the development of perturbations in time is slowed down. As an example, a shadowgram of the explosion of four tungsten wires is displayed in Fig. 4. There are virtually no perturbations along the cores, but the outer cores are approximately 20–25% thicker than the inner cores, and they are twice as large as the initial wires. The coronal plasma in the space between the wire bodies is very unstable, and a toothlike structure is seen which is most pronounced near the inner cores. Measurements of the plasma density, performed using a calibrated step tungsten attenuator,[8] showed that at the start of the discharge, up to 25–35 ns, the coronal plasma was not observed (the sensitivity threshold of the method was several percent of the initial mass), after which it became noticeable, and by 45–60 ns it reached 30–50% of the initial total mass of the load. It should be noted that according to optical measurements, both those performed a long time ago[5] and the most recent ones,[9] the behavior of the plasma in the intercore gaps changes sharply at approximately one-third of the discharge time. While the plasma initially fills the gap with electron density $10^{18}-10^{19}\ \mathrm{cm}^{-3}$ quite evenly, after 30–40 ns there arise sharply defined, dense jets directed away from the wire bodies to the discharge center.

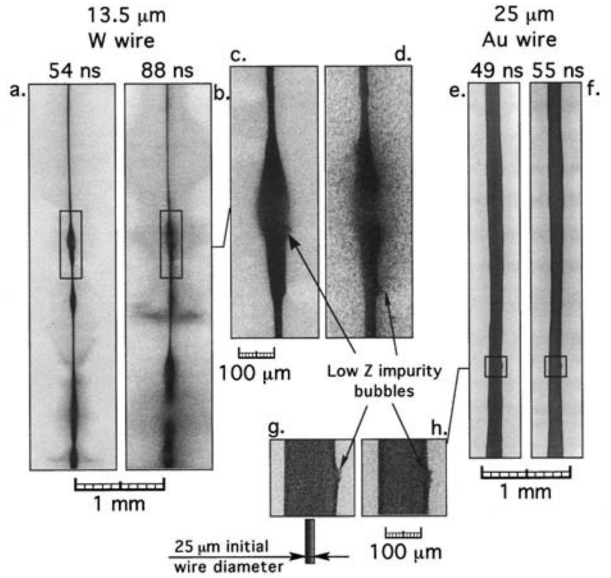

FIG. 3. Shadowgrams of discharges through W and Au wires.

We now proceed to the discussion. At the beginning of an explosion the heat release is nonuniform because of imperfections in the material and the temperature dependence of the conductivity.[1,7] The melted central part is nonuniformly superheated above the boiling point and undergoes bulk ebullition. The course of the process depends on the wire material. Parameters such as the initial conductivity, the melting and boiling temperatures, the degree of nonuniformity, and the presence of impurities are important. As the foam structure and bubbles develop, the core shows increased resistance to the current, and the voltage applied to the load continues to increase. At the same time, the surrounding vapor, whose mass is increasing, expands up to breakdown density levels. The initial state of surface is also important. As soon as electrical breakdown occurs, the corona formed engulfs the skin-layer current, and the Ohmic heating in the core vanishes, while the accumulated energy is distributed between the liquid and the vapor: The core seemingly remains in its state, having the structure of a foam column. If the energy introduced before the current vanishes were sufficient for complete vaporization of the matter, the foam structure would rapidly break down, and a vapor channel or, if the energy is even higher, a plasma channel would form at the location of the core. It is possible that this happens for easy-melting and well-conducting wires in the case of rapid current growth.

The future fate of the core depends on whether we have a load with one or many wires. In the multiwire case there are no compression waves traveling toward the core, and the core is heated only by the radiation from the corona; the liquid boils, and bubbles reach the boundary and break through it, ejecting jets of vapor into the corona. But the core remains stable, expanding slightly and evaporating from the surface. The process in a one-wire load is different: While the core awaits the arrival of the compression wave from the corona, the vapor bubbles reach a quasiequilibrium with the surrounding liquid,

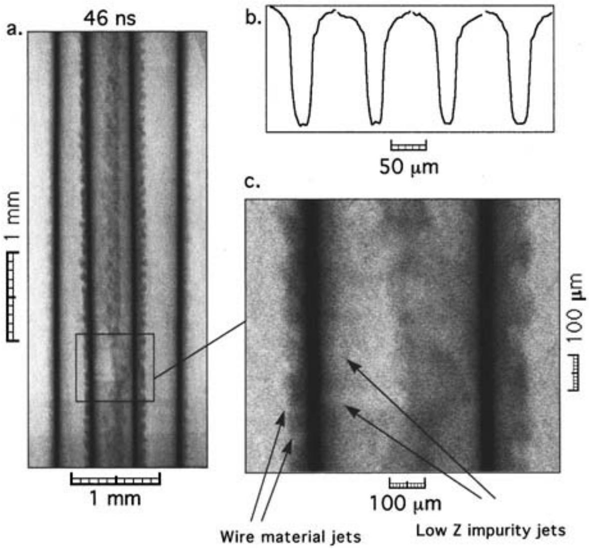

FIG. 4. Shadowgrams of a discharge through a four-wire load.

slowly ‘‘floating upward’’ under the action of the pressure gradient toward the surface of the core. Then the structure of the shock front in the core becomes manifest. The shock wave modulated by the sausage instability of the corona penetrates into the core nonuniformly, and the front, decreasing sharply in width because of the large density differential, interacts with the bubbles. The hot matter behind the shock strongly radiates, and now this determines the structure of the front in a region of width equal to the Rosseland mean free path of photons. The latter photons interact differently with the liquid and the vapor, and the presence of bubbles introduces an additional distinct feature in the radiation structure of the front: Radiation can warm only the dense liquid, leaving the temperature of the transparent vapor bubbles almost unchanged. But then the pressure in a bubble will be lower than in the bounding liquid. It is obvious that this will cause small bubbles to collapse, but the fate of the large bubbles (greater than the front width) can become different: An intense compression front, reaching their boundary, will engender an unloading wave propagating into the liquid, intensifying the vaporization. If the entropy of the unloading adiabat is lower than the entropy at the critical point, a sharp interphase boundary will remain, as one can see from the figures. As the front moves deeper, Ohmic heating of the liquid metal will also appear, which will further support vaporization. Such a bubble will grow intensely in the direction of the core surface and will ultimately break through the surface.

We shall now estimate the radiation from the compression front. It is well known[10] that in the presence of radiative heat transfer the width of the heating zone of a shock wave is given by the expression $\delta \simeq \kappa/nD \simeq (\Sigma_{SB}T^3/nD)l_R$, where D is the velocity of the front, κ is the radiative thermal conductivity, n is the atomic density, Σ_{SB} is the Stefan–Boltzmann constant, and l_R is the Rosseland mean free path of photons. In the units of the latter, this width is determined by the ratio of the radiation $\Sigma_{SB}T^4$ and hydrodynamic $n\varepsilon D$ energy fluxes (ε is the atomic internal energy). This ratio can be less than or greater than unity (subcritical and supercritical shock waves). The limiting case determines the critical temperature $T_* = (nD/\Gamma\Sigma_{SB})^{1/3}$, where Γ is the Grüneisen coefficient, which is close to 1. Taking $n \simeq 10^{22}$ cm^{-3} and $D \simeq 5\times10^5$ cm/s, we find $T_* = 12$ eV. We use for the Rosseland mean free path the estimate established in Ref. 11, viz., $l_R[\mathrm{cm}] \simeq 10^{20} T[\mathrm{eV}]/Z_n n[\mathrm{cm}^{-3}]$, which is written for a low degree of ionization (compared with the nuclear charge Z_n) and holds for transitions in both the continuous and discrete spectrum. Taking $Z_n \simeq 30$, we obtain $l_{R*} = 40$ μm and $\delta \simeq (T/T_*)^3 l_R \simeq l_{R*}(T/T_*)^4$ equals the core size $\simeq 100$ μm even at $T = 15$ eV. Here the limiting of cumulation by radiation comes into play — further focusing of the front is accompanied by an increase of not the temperature but rather the density.[12] When the wave is reflected, dense clusters of matter form near the axis. The temperature maximum shifts to this location, and a strongly nonequilibrium cellular medium consisting of a hot liquid and rapidly growing, comparatively cold and low-density, bubbles arises.

Of course, all this requires further investigations. The following facts have now been established: 1) appearance of a superheated nonequilibrium state when energy is introduced into a conductor, 2) formation of a heterogeneous core–corona structure, 3) bulk ebullition of the liquid core and transition of the core to a quasiequilibrium foamlike state, and 4) dynamic core–corona interaction. The temporal and spatial characteristics of the stages depend strongly on the parameters of the initial load and the rates of initial energy input, i.e., primarily, on the form of the current.

We thank A. R. Mingaleev for assisting in the experiment and S. Yu. Gus'kov and Ya. S. Dimant for helpful discussions. This work was partially supported by the Sandia National Laboratory (Albuquerque, USA) under contract AJ-6400.

*e-mail: ivanenkv@sci.lebedev.ru

---

[1] G. V. Ivanenkov, A. R. Mingaleev, S. A. Pikuz *et al.*, Zh. Éksp. Teor. Fiz. **114**, 1215 (1998) [JETP **87**, 663 (1998)].

[2] S. Yu. Gus'kov, G. V. Ivanenkov, A. R. Mingaleev *et al.*, JETP Lett. **67**, 559 (1998).

[3] T. A. Shelkovenko, S. A. Pikuz, A. R. Mingaleev, and D. A. Hammer, Rev. Sci. Instrum. **70,** 667 (1999).

[4] S. A. Pikuz, T. A. Shelkovenko, A. R. Mingaleev *et al.*, *Proceedings of the 12th International Conference on High-Power Particle Beams,* Haifa, Israel (1998).

[5] G. V. Ivanenkov, A. N. Lebedev, S. A. Pikuz, and S. M. Zakharov, Preprint No. 210, P. N. Lebedev Physics Institute, 1989.

[6] S. V. Lebedev, I. H. Mitchell, R. Aliaga-Rossel *et al.*, Phys. Rev. Lett. **81**, 4152 (1998).

[7] G. V. Ivanenkov, A. R. Mingeleev, T. A. Novikova *et al.*, Zh. Tekh. Fiz. **65**(4), 40 (1995) [Tech. Phys. **40**, 312 (1995)].

[8] T. A. Shelkovenko, S. A. Pikuz, A. R. Mingaleev *et al.*, Bull. Am. Phys. Soc. **43**, 1908 (1998).

[9] D. Mosher, J. R. Boller, P. P. Hinshelwood *et al.*, Bull. Am. Phys. Soc. **43**, 1642 (1998).

[10] Ya. B. Zel'dovich and Yu. P. Raĭzer, *Physics of Shock Waves and High-Temperature Hydrodynamic Processes*, Vols. 1 and 2, Academic Press, New York, 1966, 1967 [Russian original, Nauka, Moscow, 1966].

[11] V. S. Imshennik, I. N. Mikhaĭlov, M. M. Basko, and S. V. Molodtsov, Zh. Éksp. Teor. Fiz. **90**, 1669 (1986) [Sov. Phys. JETP **63**, 980 (1986)].

[12] I. V. Sokolov, Usp. Fiz. Nauk **160**(11), 143 (1990) [Sov. Phys. Usp. **33**, 960 (1990)].

Translated by M. E. Alferieff

JETP LETTERS VOLUME 69, NUMBER 5 10 MARCH 1999

Production of monochromatic radiation in an argon plasma by means of acoustic waves

A. R. Aramyan*

Institute of Applied Physics Problems, Armenian National Academy of Sciences, 375014 Erevan, Armenia

(Submitted 28 December 1998; resubmitted 4 February 1999)
Pis'ma Zh. Éksp. Teor. Fiz. **69**, No. 5, 355–357 (10 March 1999)

It is shown that monochromatic radiation ($\lambda_1 = 5888$ Å, $\lambda_2 = 5882$ Å, and $\lambda_3 = 4876$ Å) can be obtained in a gas-discharge plasma in argon with the use of acoustic waves.

[S0021-3640(99)00405-3]

PACS numbers: 52.25.Rv; 52.40.-w; 43.25.-x

Until recently, investigations of the interaction of acoustic waves with low-temperature plasma[1–6] neglected the effect of this interaction on the optical radiation spectrum of the plasma. This letter reports some experimental results on the effect of acoustic waves on optical radiation in an argon plasma.

A low-temperature argon gas-discharge plasma (pressure — 100 Torr, discharge current — 50 mA, voltage on electrodes — 2 kV) was used to study the change produced in the spectral composition of the radiation by acoustic waves. The experimental apparatus consists of a quartz discharge = tube 1000 mm long with an inner diameter of 60 mm. A high voltage with a dc current ranging from 5 to 100 mA is applied to the fingerlike electrodes. The distance between the electrodes is 850 mm. An electrodynamic sound-wave emitter is secured to one end of the tube. Light from the plasma is extracted from the other end of the tube to a spectrograph, which is used to study the change produced in the radiation spectra of the plasma by acoustic waves.

Figure 1 displays the radiation spectra of an argon plasma which were obtained using the apparatus indicated above. The radiation spectrum before the action of the acoustic waves is displayed in Fig. 1a, the radiation spectrum of the argon plasma during the action of the acoustic waves is displayed in Fig. 1b, and the radiation spectrum of the argon plasma several seconds after the action of the acoustic waves has stopped is displayed in Fig. 1c. Mercury reference lines are indicated in all figures by upward arrows. Fragments of the spectra showing the effect of the acoustic waves are presented. It is clearly seen that after the action of the acoustic waves has stopped (after ~2–3 s) intense, distinct lines with wavelengths $\lambda_1 = 5888$ Å, $\lambda_2 = 5882$ Å, and $\lambda_3 = 4876$ Å appear in the radiation spectrum of the discharge. Visually, these spectra are observed in the discharge as intense flashes with duration 15–20 ms. The flashes are observed for quite a long time (3–5 min) after the action of 180 Hz sound waves has stopped. For the most part they appear on the exterior side of the boundary of the discharge filament (near the radial boundary), where a strong change in the electron density occurs after the acoustic

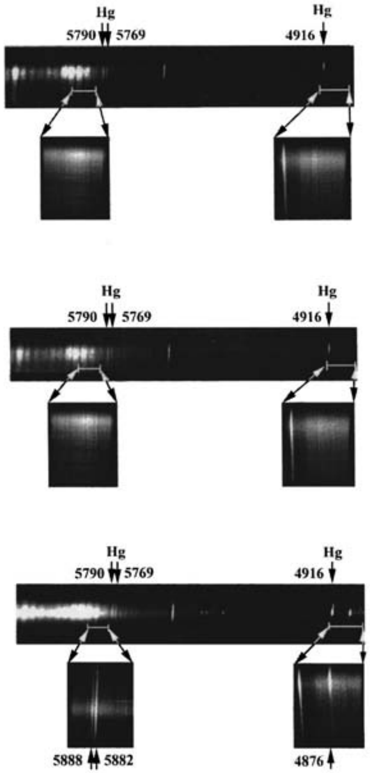

FIG. 1. Radiation spectrum of an argon plasma with pressure 110 Torr, discharge current 50 mA, and voltage on the electrodes 2 kV: a) radiation spectrum before the action of acoustic waves; b) radiation spectrum during the action of acoustic waves; c) radiation spectrum of the plasma several seconds after the action of the acoustic waves has stopped.

waves are switched off,[4,5] i.e., under the action of the acoustic waves the pinched discharge (15 mm in diameter) fills the plasma discharge chamber (which is 60 mm in diameter) more uniformly. After the acoustic waves are completely switched off, the decontracted plasma column contracts back to its initial form. Orange (5888 Å and 5882 Å) and blue (4876 Å) flashes appear in the plasma after such contraction.

Analysis of the spectral composition of the radiation in the flashes shows that the flashes correspond to three transitions on the energy levels of atomic argon:

$$7P'[1/2]_1 \rightarrow 4P[1/2]_1, \text{ wavelength } 4876\,\text{Å};$$

$$7S[3/2]_1 \rightarrow 4P[5/2]_3, \text{ wavelength} 5888\,\text{Å};$$

$$4d'[3/2]_1 \rightarrow 4P[1/2]_1, \text{ wavelength} 5882\,\text{Å}.$$

A diagram of the energy levels of these transitions in argon is presented in Fig. 2. As one can see from this figure, the oscillator strengths of the $4P \rightarrow 4S$ transitions are approximately 30–100 times greater than the oscillator strengths of the above-indicated transitions. For this reason, the $4P$ level is rapidly depopulated. As a result, a population inversion can arise between each of the levels $7P'$, $7S$, and $4d'$ on the one hand and the

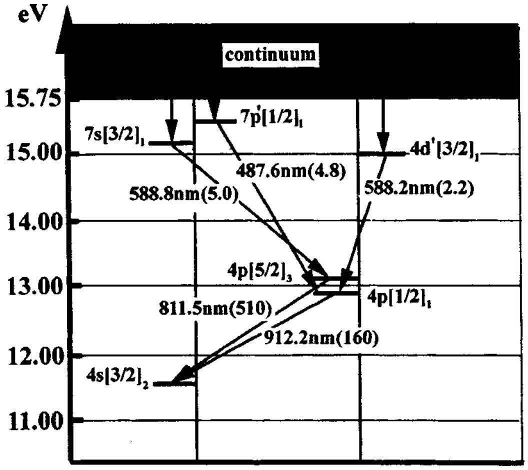

FIG. 2. Diagram of the energy levels of some transitions in argon.

4*P* level on the other. This population inversion can evidently serve at the reason for the appearance of the observed flashes. This phenomenon is probably due to relaxation processes with a long relaxation time.

I am deeply grateful to Academician A. R. Mkrtchyan for his faithful attention, consultations, and assistance in this work.

*e-mail: ara@iapp.sci.am

---

[1] U. Ingard, Phys. Rev. **145**, 41 (1966).
[2] M. Hasigawa, J. Phys. Jap. **37**, 193 (1974).
[3] A. I. Osipozh and A. V. Uvarov, Inzh.-Fiz. Zh. **55**, 149 (1988).
[4] A. R. Aramyan, G. A. Galechyan, and A. R. Mkrtchyan, Akust. Zh. **37**, 213 (1991) [Sov. Phys. Acoust. **37**, 107 (1991)].
[5] M. A. Antinyan, G. A. Galechyan, and L. B. Tavakalyan, Acoust. Phys. **82**, 619 (1996).
[6] A. R. Aramyan and G. A. Galechyan, Tech. Phys. **42**, 901 (1997).

Translated by M. E. Alferieff

JETP LETTERS VOLUME 69, NUMBER 5 10 MARCH 1999

Giant negative magnetoresistance in a nonmagnetic semiconductor

A. B. Henriques and N. F. Oliveira Jr.
Institute of Physics, University of Sao Paulo, Sao Paulo, Brazil

S. A. Obukhov and V. A. Sanina
A. F. Ioffe Physicotechnical Institute, Russian Academy of Sciences,
194021 St. Petersburg, Russia

(Submitted 15 January 1999)
Pis'ma Zh. Éksp. Teor. Fiz. **69**, No. 5, 358–362 (10 March 1999)

Studies of a classical III–V semiconductor (InSb) doped with $3d$ magnetic ions (Mn^{2+}, having a localized spin $S=5/2$) reveal some unexpected transport properties. It is found that the transition from the metallic to the low-temperature insulator phase occurs at an impurity concentration $N_{\mathrm{Mn}} \sim N_{cr} = 2\times10^{17}$ cm^{-3} and a temperature $T<T_{cr} \sim 1$ K. Under these conditions a giant negative magnetoresistance arises. The experimental results can be explained in terms of the onset of a hard Mott–Hubbard gap Δ in the impurity band formed by the shallow manganese acceptor in InSb at $N_{\mathrm{Mn}} \sim N_{cr}$. A model describing the gap formation is proposed. © *1999 American Institute of Physics.* [S0021-3640(99)00505-8]

PACS numbers: 75.30.Vn; 72.20.My

Colossal magnetoresistance and metal–insulator transitions in solid-state materials have recently come to the close attention of physicists. Such effects are typical for impurity manganites,[1] degenerate magnetic oxide semiconductors,[2] and the spin-Peierls magnetic insulator $CuGeO_3$ (Ref. 3). For all the above-mentioned materials the influence of the exchange interaction upon the crystal band structure has been found to be of great importance. The aim of the present paper is to demonstrate that similar exchange interaction effects can also be manifested in some classical nonmagnetic semiconductors doped with transition elements (in our case InSb doped with the $3d$ magnetic ions Mn^{2+}).

Our experiments were carried out on p-InSb(Mn) single crystals grown by the Czochralski method. A crystal 4 cm long and 2.5 cm in diameter had a small manganese concentration gradient from $N_{\mathrm{Mn}}=10^{17}$ cm^{-3} to 3×10^{17} cm^{-3} along the length of the crystal. Hall bars with dimensions of $(7\times1\times1)$ mm were cut from the crystal transversely to its length. This approach made it possible to study the manganese concentration dependence of the dc conductivity, magnetoresistance, and Hall effect at manganese concentrations close to N_{cr}. Temperature control was effected by means of Lake Shore Cryotronics GaAs diodes and thermistors in conjunction with He^4 and He^3 pumped

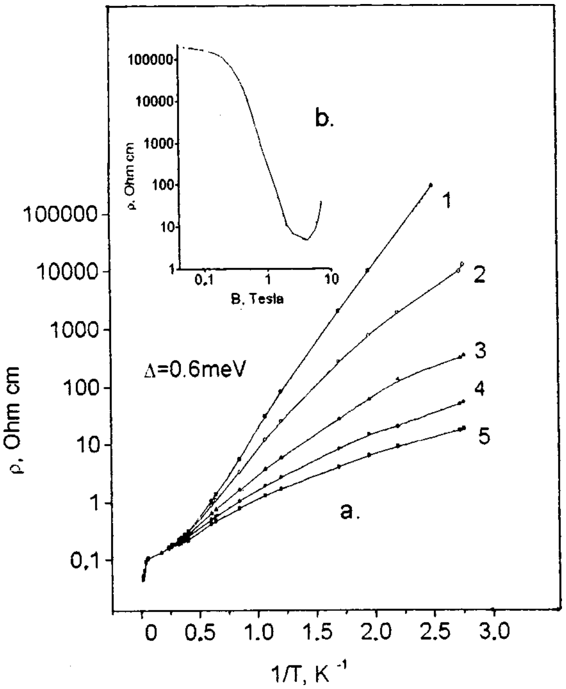

FIG. 1. a) Temperature dependence of the resistivity ρ of p-InSb(Mn) for various magnetic fields: *1* — $H=0$ ($x=0$); *2* — $H=0.5$ T ($x=0.85$); *3* — $H=1.5$ T ($x=0.75$); *4* — $H=0.5$ T ($x=0.33$). b) $\rho-H$ dependence at $T=0.4$ K. $N_{\mathrm{Mn}}=1.5\times10^{17}$ cm^{-3}.

pressure measurements. Magnetic fields of up to 7 T were induced by a superconducting magnet.

The results of the measurements (Figs. 1a and 2) demonstrate an exponential temperature dependence of the resistivity for all of the p-InSb(Mn) samples (except for the sample with the maximum manganese concentration [(Fig. 2b)] at temperatures $T<1$ K in the absence of magnetic field:

$$\rho=\rho_0\cdot\exp(\Delta/kT), \tag{1}$$

where Δ is a temperature-independent parameter which is a function of the manganese concentration and reaches its maximum value ($\Delta\simeq0.6$ meV) at $N_{\mathrm{Mn}}\sim1.5\times10^{17}$ cm^{-3}. The $\rho-T$ dependence at $N_{\mathrm{Mn}}<10^{17}$ cm^{-3} and $N_{\mathrm{Mn}}>3\times10^{17}$ cm^{-3} can be described by the variable-range hopping (VRH) conductivity equation[4]

$$\rho=\rho_0\cdot\exp(T_0/T^x), \tag{2}$$

where $x<1$, and T_0 is a temperature-independent parameter. In a magnetic field $H<3$ T and at $T<4.2$ K the resistivity decreases throughout the whole range of manganese concentration (Figs. 1 and 2). Investigation of the $\rho-T$ dependence in magnetic fields shows that increasing the magnetic field brings about a transition from the type of conductivity described by Eq. (1) to one described by Eq. (2). Thus colossal negative magnetoresistance (ρ/ρ_0) should be expected in the millikelvin temperature range if it as-

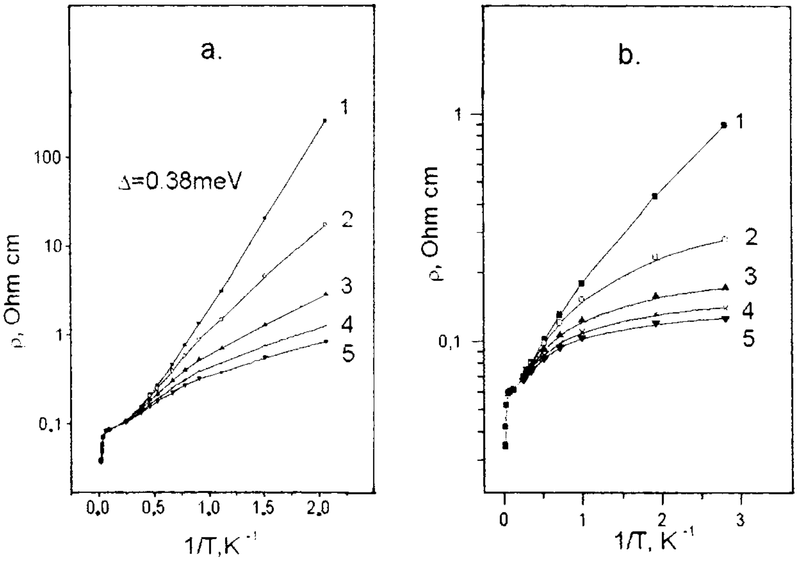

FIG. 2. Temperature dependence of the resistivity ρ of *p*-InSb(Mn) for various magnetic fields. a) $N_{\mathrm{Mn}}=1.24\times10^{17}$ cm^{-3}; *1* — $H=0$ ($x=1$); *2* — $H=0.5$ T ($x=0.75$); *3* — $H=1.0$ T ($x=0.5$); *4* — $H=1.5$ T ($x=0.33$); *5* — $H=2.0$ T ($x=0.25$). b) $N_{\mathrm{Mn}}=2.4\times10^{17}$ cm^{-3}; *1* — $H=0$ ($x=0.75$); *2* — $H=0.5$ T ($x=0.1$); *3* — $H=1.0$ T ($x=0.01$); *4* — $H=1.5$ T; *5* — $H=2.0$ T.

sumed that the value of x [in Eq. (2)] decreases twofold in a magnetic field $H\sim2$ T. It should be pointed out that the $\rho-H$ dependence has a ''shoulder'' that increases as the temperature goes down (Fig. 1b). In magnetic fields $H>3$ T the resistance increases, as is typical for the VRH conductivity in semiconductors.

In a weak magnetic field the Hall constant R_H decreases with decreasing temperature, changes sign (Fig. 3a), and increases exponentially at $T<1$ K (Fig. 3b). The R_H-T dependence is described by

$$-R_H=-R_0\exp(\Delta/kT), \tag{3}$$

where the value of Δ is the same as that of the parameter Δ obtained in the $\rho-T$ measurements [from Eq. (1)]. The high-field Hall constant ($H>3$ T) increases slightly, remaining positive as the temperature decreases.

We can understand the experimental results if it is assumed that the magnetic-impurity band in InSb(Mn) splits into two bands separated by a Mott–Hubbard gap Δ which is about 10% of the binding energy of the hole on a manganese acceptor.[5] The upper band is the electron band (negative sign of the Hall constant) and the lower band is the hole band (positive Hall constant).

The proposed model is based on a dual role of the Mn^{2+} ions.

1. Mn^{2+} ions are shallow acceptor centers ($E_a=7$ meV), giving rise to free holes in the valence band and to the formation of a narrow impurity band. These Mn^{2+} acceptor centers have a substantial qualitative influence on the characteristics of InSb, causing

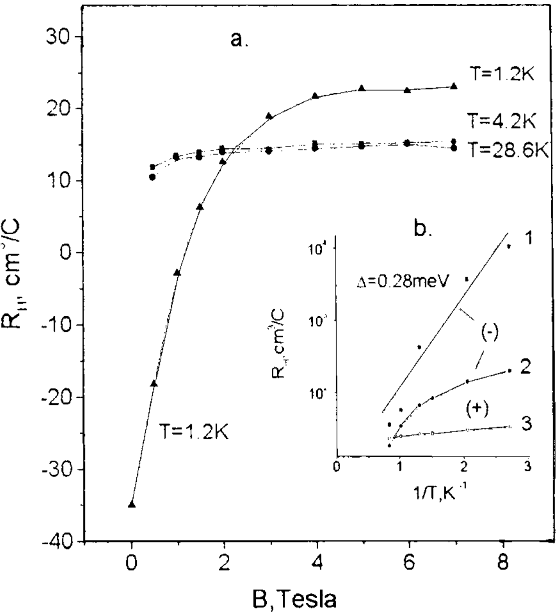

FIG. 3. Hall constant R_H as a function of magnetic field (a) and temperature (b) $N_{\mathrm{Mn}}=2.0\times10^{17}$ cm^{-3}.

effects similar to those due to nonmagnetic acceptor centers such as Ge. In InSb(Ge) single crystals free holes having uncompensated spins appear in the valence and impurity bands.[6]

We suppose that the exchange interaction between hole spins cause bounded regions with antiferromagnetically correlated spins to appear but that uniform long-range magnetic order is not formed because of the random distribution of the acceptor centers. Such a state can be characterized as a dynamic state with spin fluctuations caused by the production and decay of local antiferromagnetically correlated states. In this situation, splitting of the impurity band takes place only in bounded local regions.

2. In contrast to crystals doped with nonmagnetic impurities, in p-InSb doped with Mn^{2+} ions a magnetic system of localized spins arises. Thus an additional magnetic subsystem appears, and an exchange interaction arises between the localized Mn^{2+} ion spins ($\mathbf{S}^d$) and free-hole spins ($\mathbf{S}^p$). A uniform antiferromagnetic long-range order of the Mn^{2+} ion spins can arise due to the effective exchange interaction between $3d$ spins via spin fluctuations in the subsystem of free-hole spins — order from disorder.[7]

Let us write the spin Hamiltonian in the form

$$\mathcal{H}=\sum \mathbf{J}_{ij}^{pp}\mathbf{S}_i^p\mathbf{S}_j^p+\sum \mathbf{J}_{ij}^{pd}\mathbf{S}_i^p\mathbf{S}_j^d, \tag{4}$$

where $\mathbf{J}_{ij}^{pp}$ is the exchange interaction constant taken for free-hole spins, $\mathbf{J}_{ij}^{pd}$ is the exchange constant for the interaction between the spins $\mathbf{S}^d$ and $\mathbf{S}^p$, and i,j are the ion positions in the lattice. We assume that $\mathbf{J}_{ij}^{pp}\gg\mathbf{J}_{ij}^{pd}$. As the concentration of $3d$ ions is very

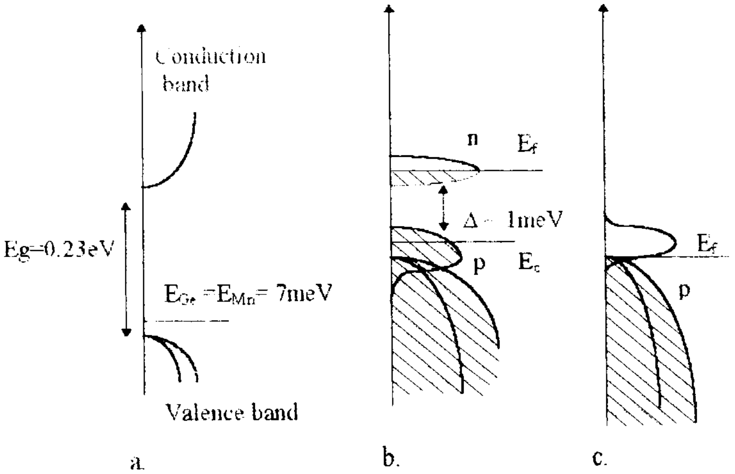

FIG. 4. Band structure of p-InSb(Mn). a) $N_{\mathrm{Mn}}=N_a \ll N_{cr}$; b) $N_a \simeq N_{cr}$; c) $N_a > N_{cr}$.

small, the direct exchange interaction between the $3d$ spins can be neglected. In the framework of perturbation theory up to second order inclusive, the effective Hamiltonian for the $3d$ ion spins can be written as

$$\mathcal{H}^{d}_{\mathrm{eff}} = \sum \mathbf{J}^{pd}_{ij} \langle \mathbf{S}^{p}_{j} \rangle \mathbf{S}^{d}_{i} + \sum (\mathbf{J}^{pd}_{ij})^2 / J^{pp}_{ij} \cdot K^{pp}_{ij} \cdot \mathbf{S}^{d}_{i} \mathbf{S}^{d}_{j}, \tag{5}$$

where $\langle \mathbf{S}^{p}_{j} \rangle$ is the spin averaged over configurati ons of free holes, and $K^{pp}_{ij} = \langle S^{p}_{i} S^{p}_{j} \rangle - \langle S^{p}_{i} \rangle \langle S^{p}_{j} \rangle$ is the spin correlation function of the holes. The first sum in the effective Hamiltonian in Eq. (5) describes the magnetization of the Mn^{2+} ion spins by the mean field $\mathbf{H}^{d}_{mf} = \Sigma \mathbf{J}^{pd}_{ij} \langle \mathbf{S}^{p}_{j} \rangle$. The value differs from zero if uniform long-range magnetic order exists in the free-hole spin subsystem.

As we have said, in the hole spin subsystem there is correlation only at finite sizes, and we have only the second sum in Eq. (5). This sum describes the effective exchange interaction of the spins $\mathbf{S}^{d}$ through correlations between hole spins. Thus the effective exchange interaction $V^{dd}_{ij} = \Sigma (\mathbf{J}^{pd}_{ij})^2 / J^{pp}_{ij} \cdot K^{pp}_{ij}$ can bring about the uniform antiferromagnetic long-range ordering of the $\mathbf{S}^{d}$ spins at a suitable ordering temperature. The internal molecular field $H_{MF} = \Sigma V^{dd}_{ij} \langle S^{d}_{j} \rangle$ arises and splits the impurity band into two bands with spins up and spins down.

Thus a hard gap of an exchange nature appears in the impurity band (see Fig. 4b). To put it in another way, a supernarrow semiconductor appears in the band gap of InSb. This hard gap can be closed in an external magnetic field H_0 due to the antiferromagnetic–ferromagnetic (spin-flip) transition when $H_0 \simeq H_{MF}$. And indeed in our case the energy Δ agrees with the value $g \mu_B H_0 \simeq 0.4$ meV at the value of the magnetic field $H_0 \sim 3$ T that provides the gap-closing effect (spin-flip effect).

The effective exchange interaction length for V^{dd}_{ij} is determined by the correlation length ξ_p of the $\mathbf{S}^{p}$ spin fluctuations. On the assumption that $\xi_p \simeq \eta_p$ (η_p is the mean free path of the holes), the V^{dd}_{ij} interaction is of the long-range type.

It is quite clear that uniform long-range ordering of the $\mathbf{S}^d$ spins can exist only at concentrations of the Mn^{2+} ions corresponding to a mean distance $\langle r\rangle \leqslant (\xi_p \simeq \eta_p)$. The equality of ξ_p and η_p correlates with a critical concentration N_{cr} and a critical temperature T_{cr} corresponding to simultaneous onset of the long-range magnetic order and the gap in the impurity band (metal–insulator transition).

[1] L. P. Gorkov, Usp. Phys. Nauk **168**, 665 (1998).

[2] E. L. Nagaev, Fiz. Tverd. Tela (St. Petersburg) **40**, 2069 (1998) [Phys. Solid State **40**, 1873 (1998).

[3] M. Hase, I. Terasaki, and K. Uchinokura, Phys. Rev. Lett. **70**, 3651 (1993).

[4] S. A. Obukhov, Fiz. Tverd. Tela. (Leningrad) **21**, 59 (1979) [Phys. Solid State **21**, 35 (1979).

[5] N. F. Mott and E. A. Davis, *Electronic Processes in Non-Crystalline Materials*, Clarendon Press, Oxford, 1979.

[6] S. A. Obukhov, in *Proceedings of the 7th International Conference on Shallow-Level Centers in Semiconductors*, edited by C. A. Ammerlaan and B. Pajot, World Scientific, 1997, p. 321.

[7] E. I. Golovenchits, B. D. Laĭkhtman, and V. A. Sanina, JETP Lett. **31**, 233 (1980); E. F. Shender, Zh. Éksp. Teor. Fiz. 326 (1982) [Sov. Phys. JETP **56**, 178 (1982).

Published in English in the original Russian journal. Edited by Steve Torstveit.

JETP LETTERS VOLUME 69, NUMBER 5 10 MARCH 1999

Effect of asymmetry of CuO_2 layers in copper oxides on the anomalous neutron scattering near T_c

V. M. Edelstein*

Institute of Solid State Physics Russian Academy of Sciences, 142432 Chernogolovka, Moscow Region, Russia

(Submitted 1 February 1999)
Pis'ma Zh. Éksp. Teor. Fiz. **69**, No. 5, 363–368 (10 March 1999)

Reasons for critical magnetic scattering of neutrons near T_c in copper oxides with CuO_2 layers whose nearest environment has no ''up–down'' symmetry are discussed. The intracrystalline electric field, which threads the CuO_2 planes on account of the asymmetry, induces coupling between the spin and momentum of the current carriers. This coupling is shown to result in a manifestation of virtual Cooper pairs in the imaginary part of the spin susceptibility. Thus spin density fluctuations as well as current fluctuations should participate in the scattering. A way of experimentally distinguishing between the two mechanisms is pointed out. © *1999 American Institute of Physics.* [S0021-3640(99)00605-2]

PACS numbers: 74.72.Bk, 61.12.Ex

The behavior of metals near superconducting phase transitions has been a topic of considerable interest during the last few decades. This field is attracting still more attention nowadays owing to the discovery of high-temperature superconductivity. The search for the mechanism responsible for this phenomenon has led to a thorough examination of conventional and unconventional behavior in every physical property and *inter alia* has stimulated reconsideration of many aspects of the order parameter fluctuations near T_c. In addition to ordinary magnetoresistivity measurements, new experimental approaches have been employed to study the problem, and one of them — inelastic neutron scattering — gives a positive result. An anomalous increase of the small-angle scattering near T_c in $YBa_2Cu_3O_{7-x}$ (YBCO) has been reported.[1] Critical neutron scattering usually occurs due to growing spin fluctuations near magnetic phase transitions. In that experiment,[1] however, the anomaly was observed near the transition to the superconductive state. Although, to the best of our knowledge, analogous experiments with single crystals have not been conducted, there can be no doubt that fluctuations of the superconducting order parameter are capable of giving rise to critical neutron scattering. Therefore, it is important to have a complete picture of the processes through which the fluctuations can affect the scattering. In the present paper we examine the role of the crystal structure of superconducting cuprates in this problem.

The magnetic field created by the magnetic moment of a neutron interacts with both the magnetic moments of the carriers (holes) and with the electric current.[2] By virtue of this, the structure factor $S(\mathbf{q},\omega)$, to which the neutron scattering intensity is proportional, has the form

$$S(\mathbf{q},\omega)=\frac{1}{\exp(\hbar\omega/k_BT)-1}\left[\chi''(\mathbf{q},\omega)+\frac{\omega}{c^2q^2}\sigma'(\mathbf{q},\omega)\right], \tag{1}$$

where χ'' is the imaginary part of the spin susceptibility and σ' is the real part of the transverse conductivity.1) Critical neutron scattering near magnetic phase transitions occurs due to critical behavior of the first term in Eq. (1). As opposed to that, in the case of a superconducting transition, it is natural to associate the anomalous scattering with the second term in the equation. Indeed, a primary source of any anomaly on approaching T_c is the formation of virtual Cooper pairs. It is known that one of two mechanisms by means of which the fluctuating Cooper pairs can affect physical quantities, the Maki–Thompson process,[3] is suppressed because of strong phase breaking (which is believed to be inherent in high-T_c superconductors), while the other, the Aslamasov–Larkin process,[4] is operative only in the conductivity but not in the susceptibility under usual conditions. Nevertheless, it will be shown below that owing to a feature of the crystal structure of some copper oxides, including YBCO, the superconducting fluctuations do give rise to a correction to $\chi''(\omega,\mathbf{q})$ which diverges at T_c just as $\sigma'(\omega,\mathbf{q})$.

This feature is the asymmetry of the nearest environment of the CuO_2 planes, to which the current carriers are confined. In the case of YBCO, the planes are surrounded by yttrium ions on the one side and by a Ba–O plane on the other side. The loss of ''up–down'' symmetry means the existence of an intracrystalline electric field threading the CuO_2 plane. For a given CuO_2 plane, the presence of the field adds the term

$$H_{so}=\frac{\alpha}{\hbar}(\mathbf{p}\times\mathbf{c})\cdot\boldsymbol{\sigma} \tag{2}$$

to the Hamiltonian of two-dimensional (2D) holes,[5] where $\mathbf{p}$, $\boldsymbol{\sigma}$, and $\mathbf{c}$ are, respectively, the 2D momentum, the Pauli matrices, and a unit vector directed along the field. Note that the coexistence of the local electric field and superconductivity is not a new fact. It was first discussed[6] in connection with A-15 compounds, the high-T_c superconductors of the 'sixties, some of which undergo a structural transition to a polar phase at a temperature T_M somewhat above the superconductin g transition T_c. Since the vectors $\mathbf{c}$ of two adjacent CuO_2 planes are oppositely directed, YBCO may be viewed as an antipyroelectric.

The following heuristic arguments show how the mirror symmetry breaking makes it possible for the superconducting fluctuations to affect χ''. Due to the Hamiltonian H_{so}, spin–velocity correlations (SVCs) appear in the system. They would be forbidden in a centrosymmetric system because velocity and spin have different transformation properties under space inversion — the former is even and the latter is odd. One of consequences of the SVC is the magnetoelectric effect (MEE) predicted earlier:[7] the supercurrent $\mathbf{J_s}$ must be accompanied by the spin polarization $\mathbf{S}$ of the carriers in an amount proportional to $\mathbf{c}\times\mathbf{J_s}$. The naive treatment of the singlet superconductor would seem to be in definite conflict with this prediction. Indeed, the singlet Cooper pair surely is not able to possess any magnetization regardless of its motion state. However, the common belief that superconductor physics is determined solely by the properties of the order parameter (the pair wave function) is incorrect for superconductors with broken mirror symmetry. In order to understand the reason for the MEE, one should remember that the off-diagonal correlation function (ODCF), $\langle \psi_\alpha(\mathbf{r})\psi_\beta(\mathbf{r}')\rangle$ (where $\psi_\gamma(\mathbf{r})$ is the electron field operator), which manifests a spontaneous breakdown of the $U(1)$ gauge invariance, is the basic conceptual element of the pairing theory,[8] and not the order-parameter matrix $\Delta_{\alpha\beta}$. Usually, in centrosymmetric systems, the spinor structure of the ODCF is identical with that of $\Delta_{\alpha\beta}$. By contrast, the band spin–orbit coupling results in the presence of a triplet part in the ODCF in addition to the singlet part even for a singlet order parameter. Moreover, it turns out that the relationship between the two parts depends on the condensate motion. It is this dependence that gives rise to the MEE. Since the neighboring CuO_2 sheets are oppositely oriented, the total magnetization equals zero. However, the mean square spin polarization due to the supercurrent fluctuations above T_c need not vanish. While the band spin–orbit coupling is caused by the local electric field, the field squared will be shown to appear in the spin fluctuations. Therefore, the contributions of all CuO_2 sheets simply add up.

The model to be calculated is based on the following premises. It is assumed that the crystal under study may be considered as a system of conducting asymmetric layers with opposite orientation of the adjacent layers and that the tunneling between the layers is negligible. It is also supposed that the electron spectrum in the absence of H_{so} and of the interparticle interaction is parabolic and isotropic, and that the singlet *s*-type pairing takes place, i.e., the Hamiltonian of one layer has the form

$$H=\int d^2r\left\{\frac{\hbar^2}{2m}\nabla\psi^+_\gamma(\mathbf{r})\cdot\nabla\psi_\gamma(\mathbf{r})+\alpha\psi^+_\beta(\mathbf{r})\left(\frac{\nabla}{i}\times\mathbf{c}\right)\cdot\boldsymbol{\sigma}_{\beta\gamma}\psi_\gamma(\mathbf{r})\right.$$
$$\left.+\frac{\lambda_s}{2}[\psi^+_\beta(\mathbf{r})g_{\beta\kappa}\psi^+_\kappa(\mathbf{r})][\psi_\delta(\mathbf{r})g_{\delta\gamma}\psi_\gamma(\mathbf{r})]\right\}, \tag{3}$$

where $\hat{g}=i\sigma_2$, and λ_s is the pairing coupling constant. The spin–orbit energy αp_F is considered to be small on the Fermi energy scale, i.e., $\alpha m/p_F\ll 1$. Then, our main result, valid for the model at $T-T_c\ll T_c$, $q\xi_{ab}(0)\ll 1$, and $l\gg\xi_{ab}(0)$ (where $l=v_F\tau$ is the mean free path and $\xi_{ab}(0)=v_F/2\pi T_c$ is the in-plane coherence length at 0 K) has the form

$$\delta\chi''_{2,ij}=(\delta_{ij}-c_ic_j)\,\delta\chi''_2,\qquad \frac{\delta\chi''_2(\omega,\mathbf{q})}{\chi_{P,2}}=\frac{\pi\omega}{8\epsilon_F}G^2_{(2)}F_2(T,\mathbf{q}), \tag{4}$$

where $\chi_{P,2}=\mu_B^2m/\pi$ is the 2D Pauli susceptibility, μ_B is the Bohr magneton, $\epsilon_F=(1/2m)p_F^2$ is the Fermi energy,

$$G_{(2)}=\frac{\alpha m}{2p_F}f_2\left(\frac{\alpha p_F}{\pi T_c}\right)$$

characterizes the coupling between the spin density and the supercurrent,

$$f_2(x)=(8/7\zeta(3))\sum_{n\geqslant 0}x^2(2n+1)^{-3}[(2n+1)^2+x^2]^{-1},$$

$\zeta(n)$ is the Riemann zeta function, the function

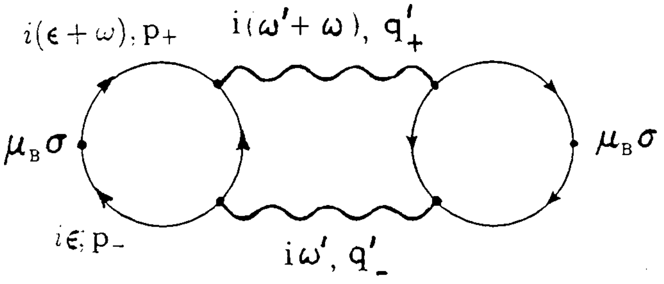

FIG. 1. The diagram for the contribution of superconducting fluctuations to the spin susceptibility. The open circle represents the three-point vertex function. The wavy lines represent the superconducting fluctuation propagator and the solid line the fermion propagator. Here $\mathbf{q}'_\pm=\mathbf{q}'\pm\mathbf{q}/2$ and $\mathbf{p}_\pm=\mathbf{p}\pm\mathbf{q}/2$.

$$F_2(T,\mathbf{q})=\frac{T_c}{T-T_c}L_2\left(\frac{\kappa_2}{2}q\xi(T)\right) \tag{5}$$

plays the role of an Ornstein–Zernike factor, $L_2(x)=[x\sqrt{1+x^2}]^{-1}\sinh^{-1}x$, $\xi(T)=\xi_{ab}(0)T_c^{1/2}(T-T_c)^{-1/2}$, $\kappa_2=[7\zeta(3)/8]^{1/2}$, and units are used in which Boltzmann’ s constant k_B and $\hbar$ are unity.

The fluctuation contribution to χ is given by the Aslamazov–Larkin type diagram shown in Fig. 1. The fermion lines represent the one-particle Green function

$$\hat{G}(i\epsilon,\mathbf{p})=\hat{\Pi}^{(+)}(\mathbf{p})[i\epsilon-\xi_{(+)}(p)]^{-1}+\hat{\Pi}^{(-)}(\mathbf{p})[i\epsilon-\xi_{(-)}(p)]^{-1}, \tag{6}$$

where the operator $\Pi^{(\pm)}_{\alpha\beta}(\mathbf{p})=1/2[\delta_{\alpha\beta}\pm(\hat{\mathbf{p}}\times\mathbf{c})\cdot\boldsymbol{\sigma}_{\alpha\beta}]$ represents projection onto states with a definite helicity (the projection of a spin on the $\mathbf{p}\times\mathbf{c}$ direction) and $\xi_{(\pm)}(p)=(p^2/2m)\pm\alpha p-\mu$ are the energies of these states. The wavy line represents the pairing fluctuation propagator $g_{\alpha\beta}D(\mathbf{q},i\omega')g_{\gamma\delta}$, where $\mathbf{q}$ is the momentum and $i\omega'$ is the frequency of the virtual Cooper pair, and the spinor indices $\alpha\beta$ and $\gamma\delta$ refer to the spin states of the carriers joining to form the pair and releasing after its subsequent decay, respectively. It can be shown that the fluctuation propagator has the usual form

$$D^{R(A)}(\mathbf{q},\omega)=-\left\{N_2(0)\left[\frac{T-T_c}{T_c}\mp\frac{i\pi\omega}{8T_c}+\frac{7\zeta(3)}{32\pi^2}\left(\frac{qv_F}{T_c}\right)^2\right]\right\}^{-1},$$

up to corrections of the order of $(\alpha p_F/\epsilon_F)^2$. Here $N_2(0)=m/2\pi$ and the superscript $R(A)$ stands for the retarded (advanced) part of the function. The most important parts of the diagram are the left and right three-point vertex functions that describe the conversion of the supercurrent density into the spin density. The functions can be found by a method pointed out earlier[7] and under the conditions mentioned above have the form

$$\mu_B(\mathbf{c}\times\mathbf{q}')\alpha m\frac{7\zeta(3)}{16\pi^3T_c^2}f_2\left(\frac{\alpha p_F}{\pi T_c}\right). \tag{7}$$

The imaginary part of the diagram comes from the product of the fluctuation propagators

$$Z(i\omega_n,\mathbf{q}'_\pm)=T\sum_\nu D(i\omega'_\nu,\mathbf{q}'_+)D(i\omega'_\nu+i\omega_n,\mathbf{q}'_-)$$

and has the standard form. Thus

$$\int \frac{q'^2 d^2 q'}{(2\pi)^2} Z''(\omega + i0^+, \mathbf{q}'_\pm) = 2\omega \left(\frac{T_c}{T - T_c} \right) \left(\frac{2\pi^3 T_c^2}{7\zeta(3)\epsilon_F} \right)^2 L_2 \left(\frac{\kappa_2}{2} q \xi(T) \right). \tag{8}$$

Equations (4) and (5) may now be obtained immediately.

Up to this point, to accentuate the main idea, we have discussed a simple model in which the the pairing interaction was considered to be the only possible interaction between carriers. However, the cuprates are highly correlated and disordered systems; narrow energy bands, strong Coulomb repulsion, and proximity to a metal–insulator transition are accepted as integral parts of the physics of cuprate superconductors. These factors affect the first and second term in Eq. (1) in opposite ways — they suppress the conductivity but enhance the ferromagnetic correlations (FMCs), which lead to a renormalization of the left and right σ-vertices of the diagram in Fig. 1. (The FMCs in the hole system must not be confused with the antiferromagnetic correlations (AFMCs) of localized spins of the copper ions.) Indeed, taking the one-site Coulomb interaction into account (in the random phase approximation) gives the quasi-Stoner factor $K = [1 - UN(0)]^{-1}$ to the vertices, U being the interaction. Then $\chi''(\omega, \mathbf{q})$ is enhanced by K^2. The unusually high relaxation rate of the planar ^{17}O nuclei, which is also mainly determined by the FMCs (the AFMCs are less active at those places), as well as the ferromagnetlike behavior of some relative copper oxides, e.g., the Na-doped La_2CuO_4 (Ref. 9) and $La_4Ba_2Cu_2O_{10}$ (Ref. 10), also points to an essential role of the FMCs in the cuprates. This assumption is consistent with the not-much-enhanced uniform susceptibility generally observed in high-T_c cuprates, because the latter contains contributions of both signs, being determined by all degrees of freedom. Now let us compare the fluctuation-induced corrections to the first and second term in Eq. (1). As $\delta\sigma' = (e^2/16) T_c / (T - T_c)$, one gets

$$\frac{\delta\chi''}{\delta\sigma'} \left(\frac{c^2 q^2}{\omega} \right) = \left[\frac{q}{p_F} \frac{m}{m_0} f \left(\frac{\alpha p_F}{\pi T_c} \right) K \frac{\alpha p_F}{4\epsilon_F} \right]^2, \tag{9}$$

where m_0 is the electron mass in the vacuum. It is seen that, at a given α, the factors that favor the relative magnitude of the first term are the low density and the heavy mass of the carriers as well as and the enhanced value of K. The minimum q in the experiment[1] was equal to $3.5 \times 10^6\ \mathrm{cm}^{-1}$, hence $qm/p_F m_0 \sim 0.3$ at $m \sim 3m_0$ (Ref. 11). A crude estimate of α in YBCO[12] has shown $\alpha p_F \sim 10^2$ K at $p_F \sim 3 \times 10^7\ \mathrm{cm}^{-1}$, i.e., one can suppose $\alpha p_F / \pi T_c \sim 1$, so that $f(\alpha p_F / \pi T_c) \sim 1$. The parameter $\alpha p_F / 4\epsilon_F$ is small, but the factor K may be large. At $K \sim 10$, both terms in Eq. (1) have the same order of magnitude.

In order to know which fraction of the neutron scattering is due to χ'', one should compare high-T_c cuprates with asymmetric (e.g., YBCO) and symmetric (e.g., $(La,Ba)_2CuO_4$) CuO_2 layers. The difference between the paraconductivities of these crystals can be determined by resistivity measurements. In principle, the value of χ'' can also be measured in experiments on magnetic field absorption. Besides the copper oxides, all that has been said above also applies to some of the superconducting ternary silicides[13] ($CeCoSi_3$ and probably $LaRhSi_3$ and $LaIrSi_3$) which crystallize in a polar structure with space group $I4mm$. They are composed of heavy elements and exhibit strong breaking of reflectional symmetry, which is suggestive of strong spin–orbit coupling.

This work was supported in part by Grant #98-02-16640 from RFBR.

*e-mail: edelsh@issp.ac.ru

1) Note that the susceptibility and conductivity in Eq. (1) are not the same quantities that appear in the Maxwell equations. To get the material χ and σ, one should, in the Feynman-diagram language, exclude from the set of diagrams for the spin−spin and current−current correlation functions those diagrams that can be cut into two parts by cutting an internal photon line. Written in terms of the material χ and σ, the right-hand side of Eq. (1) would contain additional screening factors $Z(\mathbf{q},\omega)_\chi$ and $Z(\mathbf{q},\omega)_\sigma$ in front of χ and σ, respectively. However, the differences $1-Z_{\chi,\omega}$ can be shown to be negligible under the experimental conditions.[1]

---

[1] N. R. Bernhoeft, P. J. Allen, D. McK. Paul *et al.*, Nature (London) **350**, 690 (1991).

[2] O. Halpern and M. H. Johnson, Phys. Rev. **55**, 898 (1939); see also L. L. Hirst, Rev. Mod. Phys. **69**, 607 (1997) for a more complete set of references on magnetic neutron scattering.

[3] K. Maki, Prog. Theor. Phys. **40**, 193 (1968);Thompson, Phys. Rev. B **1**, 327 (1970).

[4] L. G. Aslamazov and A. I. Larkin, Phys. Lett. A **26**, 238 (1968).

[5] This term was discussed earlier in connection with the energy spectrum of polar semiconductors; see É. I. Rashba and V. I. Sheka, Fiz. Tverd. Tela (Leningrad) **2**, 162 (1959); R. C. Gasella, Phys. Rev. Lett. **5**, 371 (1960); F. J. Ohkawa and Y. Uemura, J. Phys. Soc. Jpn. **37**, 1325 (1974).

[6] P. V. Anderson and E. I. Blount, Phys. Rev. Lett. **14**, 217 (1965).

[7] V. M. Edelstein, Phys. Rev. Lett. **75**, 2004 (1995).

[8] J. Bardeen, L. N. Cooper, and J. R. Schrieffer, Phys. Rev. **106**, 162 (1957).

[9] M. A. Subramanian, J. Gopalakrishnan, C. C. Torardi *et al.*, Science **240**, 495 (1988).

[10] H. Masuda, F. Mizuno, I. Hirabayashi, and S. Tanaka, Phys. Rev. B **43**, 7871 (1991).

[11] D. R. Harshmann and A. P. Mills, Phys. Rev. B **45**, 10684 (1992).

[12] V. M. Edelstein, Phys. Rev. Lett. **80**, 5766 (1998).

[13] P. Haen, P. Lejay, B. Chevalier *et al.*, J. Less-Common Met. **110**, 321 (1985).

Published in English in the original Russian journal. Edited by Steve Torstveit.

JETP LETTERS VOLUME 69, NUMBER 5 10 MARCH 1999

Macroscopic coherent tunneling in a small particle of an uncompensated antiferromagnet in a strong magnetic field

B. A. Ivanov and V. E. Kireev
Institute of Magnetism, Ukrainian National Academy of Sciences, 252142 Kiev, Ukraine

(Submitted 10 December 1998; resubmitted 2 February 1999)
Pis'ma Zh. Éksp. Teor. Fiz. **69**, No. 5, 369–374 (10 March 1999)

A new macroscopic quantum tunneling effect is predicted for a particle of an uncompensated ferritin-type antiferromagnet in a noncollinear phase induced by a strong magnetic field. © *1999 American Institute of Physics.* [S0021-3640(99)00705-7]

PACS numbers: 75.50.Ee, 75.45.+j

The phenomenon of macroscopic quantum tunneling (MQT) in magnets has been widely studied in recent years, both experimentally and theoretically. Special attention has been devoted to coherent MQT (CMQT) — the phenomenon of tunneling between energetically equivalent but macroscopically different states, so that a quantum superposition of nearly classical states of a magnet can occur (see, for example, Refs. 1–3). This interest is due to two factors. First, in this case tunneling can be observed directly according to resonance absorption on split levels. Second, subtle and beautiful effects due to destructive interference arise in the analysis of CMQT, for example, a dependence of the magnetization tunneling probability on whether the total spin of a particle is an integer or half-integer. However, these effects are much more difficult to observe than, for example, quantum magnetic relaxation (depinning of walls), and we know of only several works where they have been observed.[4,5] In these works small antiferromagnetic ferretin particles, containing approximately 4500 magnetic iron ions with approximately 50 uncompensated spins, were used. Previously discussed MQT effects in small particles of a ferromagnet and an uncompensated antiferromagnet (AFM) have always led to the appearance of one resonance absorption line. Under conditions allowing the observation of this line (sufficiently low temperatures, absence of a magnetic field) it is virtually impossible to find a parameter whose variation would control the position of this line. This makes it difficult to give an unequivocal interpretation of the line. The oscillatory dependence, discussed in Refs. 6–8, of the tunneling probability in small magnetic particles on the external magnetic field appeared to afford a good opportunity for checking whether the observed line is indeed caused by CMQT. But this effect existed only for a completely compensated AFM (otherwise a magnetic field completely lifts the degeneracy in the system), even if the orientation of the field relative to the crystallographic axes is strictly determined. It is clear that these conditions cannot be realized for an ensemble consisting a large number of small ferretin-type AFM particles in which the sublattice spins are not completely compensated (on account of the effect of the surface, at least).

In the present letter we shall discuss CMQT effects of a new type for a freely rotating AFM particle with incomplete spin compensation in an external field. The main feature of this effect is that in the sufficiently strong field the sublattice magnetizations are noncollinear and the field orients the particle in such a way that twofold degeneracy of the classical ground state can appear in the system. The height of the tunneling barrier and the phase factor of the tunneling amplitude depend strongly on the intensity of the field. This makes it possible to control the tunneling probability by varying the field.

Let us consider a spin system where the nearest neighbors are coupled by an antiferromagnetic interaction. We shall assume that all lattice sites occupied by spins can be divided into two groups in such a way that the member spins of pairs of nearest neighbors belong to different groups and there are no frustrations. For an ideal AFM these two groups correspond to two magnetic sublattices. We write the Hamiltonian of such a system, taking account of the uniaxial anisotropy and the external magnetic field **H**, in the form

$$\hat{H}=J\sum_{\mathbf{r},\mathbf{r}'}\mathbf{S}_{\mathbf{r}}\cdot\mathbf{S}_{\mathbf{r}'}+K\left[\sum_{\mathbf{r}}(S^z_{\mathbf{r}})^2+\sum_{\mathbf{r}'}(S^z_{\mathbf{r}'})^2\right]-g\mu_B\mathbf{H}\cdot\left(\sum_{\mathbf{r}}\mathbf{S}_{\mathbf{r}}+\sum_{\mathbf{r}'}\mathbf{S}_{\mathbf{r}'}\right). \tag{1}$$

Here J is the exchange integral; the vectors $\mathbf{r}$ and $\mathbf{r}'$ enumerate the sites of the first and second groups, respectively; $K>0$ is an easy-plane anisotropy constant; g is the gyromagnetic ratio; μ_B is the Bohr magneton; **H** is the magnetic field; and, the summation in the first term extends only over pairs of nearest neighbors. We shall assume that the anisotropy energy is small compared with the exchange energy. This corresponds to the inequality $K\ll J$. For simplicity, all spins are assumed to be identical (i.e., all spins have the same magnitude, g factor, anisotropy constant, and so on). The generalization to the case of nonequivalent spins for the approximation employed above (uniform rotation of the sublattice magnetizations) does not present any difficulties.

Let us discuss the ground state of this system. It is obvious that when only the exchange interaction and anisotropy are taken into account the spins in each of the two groups of sites become oriented antiparallel to one another, forming total sublattice spins $\mathbf{S}_1=\Sigma_{\mathbf{r}}\mathbf{S}_{\mathbf{r}}$ and $\mathbf{S}_2=\Sigma_{\mathbf{r}'}\mathbf{S}_{\mathbf{r}'}$ lying in the easy plane. Such an orientation will remain even for an uncompensated AFM. However, the effect of a magnetic field is substantially different for the case of a compensated AFM and for $S_1\neq S_2$.

Indeed, for $S_1\neq S_2$ (for definiteness let $S_1>S_2$), in the exchange approximation the system possesses a nonzero magnetic moment. This moment will strive to align itself in a direction parallel to the field, i.e., in such a way that $\mathbf{S}_1$ is parallel and $\mathbf{S}_2$ antiparallel to the field. In addition to this ferrimagnetic effect, which is linear in **H**, there exists another orientational effect of a magnetic field which also appears for $S_1=S_2$. This effect is due to the fact that the susceptibility of the AFM is maximum in a direction perpendicular to $\mathbf{S}_1$ and $\mathbf{S}_2$. This effect is quadratic in **H**, and in weak fields it plays a small role. As is well known, as a result of this, states in which the sublattices are noncollinear can arise in an uncompensated ferrimagnetic (see, for example, Ref. 7). The same situation occurs here. It is obvious that $\mathbf{S}_1$ and $\mathbf{S}_2$ will lie in the easy plane and the particle will become oriented under the action of a field in such a way that the easy plane will be parallel to the field. Then the ground state is determined by the angles θ_1 and θ_2 between $\mathbf{S}_1$ and $\mathbf{S}_2$ and the field. The values of these angles can be found by minimizing the sum of the Zeeman and exchange energies. An elementary analysis of Eq. (1) shows that for $H \leqslant H_c$ or $H \geqslant H_e$, where

$$H_c = \frac{Js^2 N_z S_{\rm ex}}{g\mu_B S_1 S_2}, \quad H_e = \frac{Js^2 N_z S_{\rm tot}}{g\mu_B S_1 S_2} \tag{2}$$

(here N_z is the number of nearest-neighbor pairs, s is the site spin, $S_{\rm ex} = S_1 - S_2$ is the uncompensated particle spin, and $S_{\rm tot} = S_1 + S_2$ is the total spin), the sublattice spins are collinear to one another and to $\mathbf{H}$. For $H < H_c$ the angles $\theta_1 = 0$, $\theta_2 = \pi$, and for $H > H_c$ one has $\theta_1 = \theta_2 = 0$. In this case the classical ground state of a particle is nondegenerate and there are no coherent MQT effects. However, for $H_c < H < H_e$ the spins $\mathbf{S}_1$ and $\mathbf{S}_2$ are noncollinear. The total magnetic moment is parallel to $\mathbf{H}$, i.e., $S_1 \sin\theta_1 + S_2 \sin\theta_2 = 0$, but the state of the system is twofold degenerate with respect to the signs of the projections of $\mathbf{S}_1$ and $\mathbf{S}_2$ on a direction perpendicular to $\mathbf{H}$ and lying in the easy plane.

For $S_1 \approx S_2$, the case of interest to us, the field $H_e \simeq 2JZs/g\mu_B$, where $Z = 2N_x s/S_{\rm tot}$ is the effective number of nearest neighbors, is identical in value to the exchange field of the AFM, and $H_c = H_e S_{\rm ex}/S_{\rm tot} \ll H_e$. Therefore the ground state of the particle is twofold degenerate in a wide range of fields, and coherent MQT effects are possible. For ferretin particles it can be assumed that $S_1 \simeq S_2 \simeq 5 \times 10^3$, $S_{\rm ex} \simeq 50$, and $H_e \simeq 10^4$ kOe (Ref. 5), which gives $H_c \simeq 50$ kOe. We shall confine our analysis to the case $H_c \leqslant H \ll H_e$. For $H \ll H_e$ the vectors $\mathbf{S}_1$ and $\mathbf{S}_2$ are approximately antiparallel and the total spin $\mathbf{S}_1 + \mathbf{S}_2$ is small compared to the difference $\mathbf{S}_1 - \mathbf{S}_2$, $|\mathbf{S}_1 + \mathbf{S}_2| \ll |\mathbf{L}|$, and $\mathbf{L} = \mathbf{S}_1 - \mathbf{S}_2$. In this case the dynamics of an AFM can be described on the basis of a generalization of the well-known nonlinear σ model to uncompensated AFMs, which has been done for classical magnets[9] and for the quantum case using spin coherent states.[10] In this model the dynamic variable is the unit vector $\mathbf{l} = \mathbf{L}/|\mathbf{L}|$, and the magnetization is determined by the magnitude of the magnetic field and by $\mathbf{l}$ and $\partial\mathbf{l}/\partial t$ (see Refs. 9 and 10).

We shall write the Euclidean Lagrangian for the vector $\mathbf{l}$ in angular variables as

$$\mathcal{L} = -i\hbar S_{\rm tot}\dot{\varphi} + i\hbar S_{\rm ex}\dot{\varphi}\cos\theta + \frac{\hbar S_{\rm tot}}{\gamma H_e}\left[\frac{1}{2}(\dot{\theta}^2 + \sin^2\theta\dot{\varphi}^2) - i\gamma H\dot{\varphi}\sin^2\theta\right] + W_{\rm st}. \tag{3}$$

Here $\mathbf{H}$ is directed along the quantization axis z, $\gamma = g\mu_B/\hbar$, a dot denotes differentiation with respect to the imaginary time $\tau = it$, and $W_{\rm st}(\theta, \varphi)$ is the static energy of a particle written in terms of the vector $\mathbf{l}$ (see below). This Lagrangian differs from the Lagrangian given previously in Ref. 10 only by the term $i\hbar(S_{\rm ex} - S_{\rm tot})\dot{\varphi} = -2sN_z i\hbar\dot{\varphi}$, which is a total derivative. For the previously[11] studied instanton solutions, in which the change in the angle $\varphi = \pi$, it reduces to $2\pi is\hbar N_z$ and is a multiple of $i\pi\hbar$ for both integer and half-integer spins, which does not change the tunneling probability. However, in our case, where the change in φ can be different from π, it is important to take this term into account. The character of the distribution $\mathbf{l}(\tau)$ in the instanton solution is determined by the form of the static energy, which it is convenient to represent as

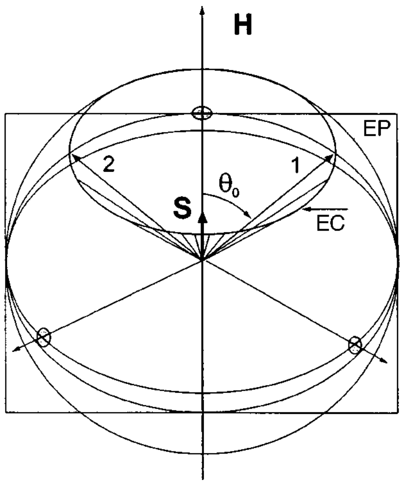

FIG. 1. Relative arrangement of the magnetic-field vector **H**, the total-spin vector **S**, and the vector **l** in two states (denoted as 1 and 2). EP — easy plane, EC — easy cone, $\cos\theta_0 = H_c/H$.

$$W_{\mathrm{st}} = \frac{(g\mu_B S_{\mathrm{tot}})^2}{8JN_z s^2}(\mathbf{H}\cdot\mathbf{l} - H_c)^2 + KsS_{\mathrm{tot}}(\mathbf{l}\cdot\mathbf{n})^2, \tag{4}$$

where **n** is the hard axis. Here the first term determines the interaction energy between **l** and the magnetic field, and the second term gives the anisotropy energy. This formula makes it possible to represent clearly the character of the ground state of an uncompensated AFM as well as the scale of variation of the energy away from the ground state (see Fig. 1). The vector **l**, directed along the generator of a cone with half-angle $\theta_0 = \cos^{-1}(H_c/H)$ and axis in the direction of **H**, $\mathbf{l}\cdot\mathbf{H} = H_c$, corresponds to the minimum for the first term for $H > H_c$. The condition that **l** lies in the easy plane, $\mathbf{l}\perp\mathbf{n}$, corresponds to a minimum of the second term. Since a free particle becomes oriented so that the field **H** also lies in the easy plane, two directions formed by the intersection of the cone $\mathbf{l}\cdot\mathbf{H} = H_c$ and the easy plane $\mathbf{l}\cdot\mathbf{n} = 0$ correspond to the ground state for $H_c < H < H_e$. The two terms in W_{st} become of the same order of magnitude in the field

$$H_* = \frac{2s}{g\mu_B}\left(\frac{2JN_z Ks}{S_{\mathrm{tot}}}\right)^{1/2} \sim H_e\left(\frac{K}{J}\right)^{1/2}.$$

For a compensated particle of a weakly anisotropic magnet, the case of interest to us, H_*, just as that of H_c introduced above, is small compared to H_e, though the ratio of H_* and H_c can be arbitrary. According to the estimates made in Ref. 5, for a ferretin particle $H_* \simeq H_c$.

Exact instanton solutions can be constructed in the two limiting cases $H \gg H_*$ and $H \ll H_*$ (naturally, in the second case it is assumed that $H_c < H$, i.e., $H_e \ll H_*$). For $H \gg H_*$ the interaction with the magnetic field is the determining factor, so that **l** moves near the cone $\mathbf{l}\cdot\mathbf{H} = H_c$, and the anisotropy creates a barrier through which tunneling occurs. In the opposite case, $H_c < H \ll H_*$, **l** moves in the easy plane $\mathbf{l}\cdot\mathbf{n} = 0$ and the magnetic field creates the barrier.

We start with the more interesting situation of weak anisotropy $H \gg H_*$. In this case the instanton trajectory will lie near the cone $\theta = \theta_0$. We introduce the deviation from the cone — the small angle $\vartheta = \theta - \theta_0$. In the leading order approximation in H_*/H the angle ϑ can be expressed in terms of φ and $\dot{\varphi}$. Eliminating θ from Eq. (3), we can write an effective Lagrangian that depends only on one dynamical variable — the azimuthal angle φ:

$$\mathcal{L}_{\mathrm{eff}} = -i\hbar S_{\mathrm{tot}}\dot{\varphi} + i\hbar S_{\mathrm{ex}}\frac{H_c}{H}\dot{\varphi} - i\hbar S_{\mathrm{tot}}\frac{H}{H_e}\left(1-\frac{H_c^2}{H^2}\right)\dot{\varphi}$$

$$+\frac{\hbar S_{\mathrm{tot}}}{2\gamma H_e}\sin^2\theta_0[\dot{\varphi}^2(1+9k^2\cot^2\theta_0)+(k\gamma H_*\cos\varphi)^2]. \qquad (5)$$

Here $k = 4S_1S_2/S_{\mathrm{tot}}^2 \approx 1$. In what follows we shall set $k=1$. The correction $9\cot^2\theta_0$ to the effective mass is due to the deviation of the trajectory away from the cone and contains contributions both from the gyroscopic interaction of **l** with the field and from the uncompensated spin. This correction predominates for $\theta_0 \ll 1$ ($H \to H_c$), which is possible if $H_c \gg H_*$, i.e., $S_{\mathrm{ex}}/S_{\mathrm{tot}} \gg (K/J)^{1/2}$. In this case, as is well known,[9] the dynamics is of a ferromagnetic character. At the same time, at $\theta_0 \simeq \pi/2$ ($H \gg H_c$) this correction is small, which corresponds to the antiferromagnetic limit. Since $H \gg H_*$, this inequality means that in the presence of a magnetic field antiferromagnetic dynamics can be realized for any ratio of H_c and H_* (or, in other words, between $S_{\mathrm{ex}}/S_{\mathrm{tot}}$ and $\sqrt{K/J}$) and, as noted in Ref. 9, the condition for it to be realized is $S_{\mathrm{ex}}/S_{\mathrm{tot}} \ll \sqrt{K_{\mathrm{eff}}/J}$, where $K_{\mathrm{eff}} = K + (g\mu_B H)^2/8J$.

It is easy to represent the instanton solutions for the Lagrangian (5) in the form

$$\cos\varphi = \pm\frac{1}{\cosh\Omega\tau} \quad \text{and} \quad \Omega = \frac{\gamma H_*}{\sqrt{1+9\cot^2\theta_0}}. \qquad (6)$$

The Euclidean action for these solutions can be written as

$$\mathcal{A}_{eu} = \hbar(A \pm i\Phi), \qquad (7)$$

where

$$\Phi = -\pi S_{\mathrm{tot}} + \pi S_{\mathrm{ex}}\left(2\frac{H_c}{H} - \frac{H}{H_c}\right) \quad \text{and} \quad A = 2S_{\mathrm{tot}}\frac{H_*}{H_e}\frac{\sin^3\theta_0}{\sqrt{1+8\cos^2\theta_0}}. \qquad (8)$$

The tunneling rate is determined by the sum of the amplitudes corresponding to two instanton solutions [the + and − signs in Eq. (7)]:

$$\Gamma = 8\pi\Omega A^{1/2}\left|\cos\left[\pi S_{\mathrm{ex}}\left(2\frac{H_c}{H} - \frac{H}{H_c} - 1\right)\right]\right| \exp\left(-2S_{\mathrm{tot}}\frac{H_*}{H_e}\frac{\sin^3\theta_0}{\sqrt{1+8\cos^2\theta_0}}\right), \qquad (9)$$

where an unimportant term $2\pi S_{\mathrm{tot}}$ has been dropped in the argument of the cosine. The real part of the action that is proportional to the total spin differs from the analogous expression for a pure AFM by a numerical factor that depends on θ_0 (Ref. 7). This factor is of the order of unity for $\theta_0 \sim 1$, and as $\theta \to 0$ ($H \to H_c$) it approaches zero as θ_0^3, i.e., as $[(H-H_c)/H_c]^{3/2}$. The phase term depends strongly on the magnetic field H. Characteristically, the prohibition on tunneling that occurs for a compensated AFM with half-integer S_{ex} is absent. The phase factor $\mathbf{\Phi}$ increases monotonically with H, and the transition probability is an oscillatory function of the field with characteristic period $\Delta H = H_c H^2 [S_{\text{ex}}(H^2+2H_c^2)]^{-1}$, which depends on the magnitude of the field. For $H \sim H_c$ we have $\Delta H \simeq H_c/S_{\text{ex}}$, which can be small compared with H_c. For ferretin particles $\Delta H \simeq 1$ kOe.

For $H_c < H \ll H_*$ the instanton trajectory lies in the easy plane, and there are no destructive interference effects. The correction to the instanton mass, analogous to $9\cot^2\theta_0$ (5), is an infinitesimal of the order of $(H_c/H_*)^2$, and the dynamics is of an antiferromagnetic character. The real part of the action is determined by the formula $A_2 = 2S_{\text{tot}}(\sin\theta_0 - \theta_0\cos\theta_0)H/H_e$. In the intermediate region $H \sim H_*$ both the real and imaginary parts of $\mathbf{l}$ must be taken into account and an exact solution cannot be constructed, but it is not difficult to analyze the qualitative behavior of the tunneling probability. In this case, just as for $H \gg H_*$, there exist two instanton trajectories for Re$\mathbf{l}$ which pass inside the cone $\cos\theta = H_c/H$ and are symmetric relative to the easy plane. They correspond to the same values of Re$\mathcal{A}_{eu}$, and the values of Im$\mathcal{A}_{eu}$ differ only in sign. Therefore Eq. (9) is qualitatively applicable for $H \gtrsim H_*$ as well.

This work is supported by a grant from the Ukrainian Fund for Fundamental Studies 2.4/27 ‘‘Tunnel’.’’

[1] L. Gunther and B. Barbara (Eds.), *Quantum Tunneling of Magnetization*, Vol. 301, NATO ASI Series E, Kluwert, Dordrecht, 1995.

[2] E. M. Chudnovsky and J. Tejada, *Macroscopic Quantum Tunneling of the Magnetic Moment*, Cambridge University Press, 1988.

[3] B. A. Ivanov and A. K. Kolezhuk, in *Frontiers in Magnetism of Reduced Dimension Systems*, edited by V. G. Bar’yakhtar, P. E. Wigen, and N. A. Lesnik, Vol. 49, NATO ASI Series 3, High Technology, Kluwert, Dordrecht, 1988.

[4] D. D. Awschalom, J. F. Smyth, G. Grinstein *et al.*, Phys. Rev. Lett. **68**, 3092 (1992).

[5] J. Tejada, X. X. Zhang, E. del Barco *et al.*, Phys. Rev. Lett. **79**, 1754 (1997).

[6] E. N. Bogachek and I. V. Krive, Phys. Rev. B **46**, 14559 (1992).

[7] V. Yi. Golysev and A. F. Popkov, Europhys. Lett. **29**, 237 (1995); Zh. Éksp. Teor. Fiz. **108**, 1755 (1995) [JETP **81**, 962 (1995)].

[8] A. Chiolero and D. Loss, Phys. Rev. Lett. **80**, 169 (1998).

[9] B. A. Ivanov and A. L. Sukstanskii, Solid State Commun. **50**, 523 (1984); Zh. Éksp. Teor. Fiz. **84**, 370 (1983) [Sov. Phys. JETP **57**, 214 (1983)].

[10] A. Chiolero and D. Loss, Phys. Rev. B **56**, 738 (1997).

[11] K. P. Belov, A. K. Zvezdin, A. M. Kadomtseva, and R. Z. Levitin, *Orientational Transitions in Rare-Earth Magnets*, Nauka, Moscow, 1979.

Translated by M. E. Alferieff

JETP LETTERS VOLUME 69, NUMBER 5 10 MARCH 1999

Magnetically two-phase state in $Eu_{1-x}A_xMnO_3$ (A=Ca, Sr)

A. I. Abramovich, R. V. Demin, L. I. Koroleva,* A. V. Michurin,
and A. I. Smirnitskaya
M. V. Lomonosov Moscow State University, 119899 Moscow, Russia

(Submitted 28 December 1998; resubmitted 3 February 1999)
Pis'ma Zh. Éksp. Teor. Fiz. **69**, No. 5, 375–380 (10 March 1999)

It is observed that low-temperature magnetic properties (dependence of the magnetization on the cooling conditions and the presence of a maximum in the initial magnetic susceptibility) of $Eu_{1-x}A_xMnO_3$ (A=Ca, Sr; $x=0,0.3$) samples are similar to those of spin glasses. However, there are also substantial differences: The magnetization depends on the cooling conditions right up to the maximum measurement fields $H=45$ kOe, and the temperature of T_N of the maximum of the initial magnetic susceptibility is independent of the frequency of the ac magnetic field in which the susceptibility is measured. The magnetization isotherms for $T \leqslant T_N$ are a superposition of a linear part, characteristic for an antiferromagnet, and a small spontaneous part. For compositions containing Sr a maximum of the resistivity ρ ($\rho_{\max} \sim 10^8\ \Omega \cdot \mathrm{cm}$) is observed near T_N; in a 120 kOe magnetic field this maximum is lowered by four orders of magnitude and the temperature of the maximum is two times higher. In compositions with $x=0.3$ the paramagnetic Curie point is much higher than for the composition with $x=0$: $\theta=110$ K (A=Ca), 175 K (A=Sr), and -100 K ($x=0$). These characteristic features of the magnetic and electric properties are explained by the existence of a magnetically two-phase state in this system, consisting of ferromagnetic clusters, in which the charge carriers are concentrated, embedded in an insulating antiferromagnetic matrix. © *1999 American Institute of Physics.* [S0021-3640(99)00805-1]

PACS numbers: 75.60.Ej, 75.30.Cr, 75.30.Kz

In recent years interest in manganese oxide compounds with the perovskite structure and the chemical formula $Re_{1-x}A_xMnO_3$ (Re=La and rare-earth elements; A=Ca, Sr, Ba) has increased sharply because of the colossal magnetoresistance (CMR) observed in some of them at room temperature. These materials have already found application in diverse sensing devices. However, there is a difference of opinion as to the nature of their CMR (see, e.g., the review articles[1,2] and the references cited therein). The problem is that compared with ordinary magnetic semiconductors, where the CMR is explained by the existence of strong $s-d$ exchange and the magnetically two-phase state induced by such exchange, the picture in manganites is more complicated because of the existence of the Jahn–Teller effect and the relative softness of the lattice, as a result of which the lattice type changes under the action of a magnetic field, pressure, and temperature. On this basis a number of authors have advanced other hypotheses to explain the characteristic features of the resistivity ρ and CMR in manganites, for example, a transition from hopping to polar type conductivity near the Curie point T_C, melting of a charge-ordered state under the action of a magnetic field, and others. However, it should be noted that just as in ordinary magnetic semiconductors the maxima of ρ and CMR in manganites are observed near T_C, and the CMR consists in the suppression of the peak in ρ near T_C. It is impossible to explain this experimental fact on the basis of the hypotheses indicated above. We propose that the characteristic features of ρ and CMR in manganites near T_C are of the same nature as in ordinary semiconductors, specifically, they are due to strong $s-d$ exchange and the magnetically two-phase state caused by such exchange.[1] We shall show this for $Eu_{1-x}A_xMnO_3$ (A=Ca, Sr; $x=0, 0.3$).

There are only a few works devoted to the study of this system.[3–8] In these works it was observed that compositions with $x=0$, 0.3 (A = Ca, Sr) and 0.42 (A= Sr) possess semiconducto r-type conductivity and compositions with Ca and Sr possess a CMR.[7,8] The $x=0$ composition is an antiferromagnet (with Néel temperature $T_N\approx 40$ K) in which ferromagnetic (FM) clusters are present. The volume of the FM phase increases with increasing Eu deficiency or O excess.[5,6] The nature of the FM clusters is not discussed in Refs. 5 and 6. It is merely indicated that a large magnetic anisotropy exists inside the FM clusters. In Refs. 5 and 7 it is hypothesized that a spin-glass (SG) state occurs in $Eu_{1-x}A_xMnO_3$ (A=Ca, Sr).

To clarify the nature of the FM phase in $Eu_{1-x}A_xMnO_3$ (A=Ca, Sr), in the present work we studied the temperature dependence of the magnetization M in weak and strong magnetic fields, the initial magnetic susceptibility χ in an ac magnetic field with frequency ranging from 0.8 to 8 kHz, the paramagnetic susceptibility, the resistivity ρ, and the magnetoresistance $\Delta\rho/\rho$. The production of ceramic samples with $x=0$ and 0.3 and their analysis and crystal structure are described in Ref. 8. The magnetization measurements were performed by the ballistic method; the initial magnetic susceptibility in an ac magnetic field with frequency from 0.8 to 8 kHz was measured with a F-5063 ferrometer and the paramagnetic susceptibility was measured using a balance (weighing) method with electromagnetic compensation. The electric resistance was measured by a four-probe method, using a Keithley-182 nanovoltmeter with 19 $g\cdot\Omega$ input resistance; indium contacts to the sample were made using an ultrasonic solderer.

It was found that for all compositions studied the low-temperature magnetization depends on the conditions under which the sample is cooled. As an example, the temperature dependence of the magnetization in the weak magnetic field $H=58$ Oe for a $Eu_{0.7}Ca_{0.3}MnO_3$ sample is displayed in Fig. 1. The $M(T)$ curve of a sample cooled in a zero magnetic field possesses a maximum in a weak field 58 Oe at temperature T_f, while there is no maximum on the $M(T)$ curve of the sample cooled in this field (the magnetization was measured with cooling in a nonzero field) and the magnetization increases monotonically with decreasing temperature. The magnetization at 4.2 K for a sample cooled in a nonzero field reaches values which are approximately an order of magnitude greater than the value of M for the sample cooled in a zero magnetic field. It is evident from the inset in Fig. 1 that the sample cooled in a nonzero field has a magnetization hysteresis loop shifted along the H axis, while for the sample cooled in a zero field the hysteresis loop is essentially symmetric. The magnetic properties presented above seemingly attest to the existence of a cluster SG state or superparamagnetism below T_f.

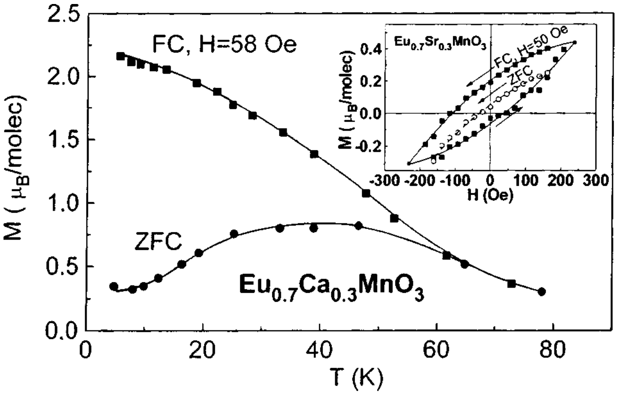

FIG. 1. Temperature dependence of the magnetization of $Eu_{0.7}Ca_{0.3}MnO_3$ in a weak magnetic field. Inset: Hysteresis loop of a $Eu_{0.7}Sr_{0.3}MnO_3$ sample cooled in nonzero and zero fields.

However, in this case the magnetization of the sample cooled in a nonzero field should not depend on T for $T < T_f$, if the size of the magnetic clusters does not change with temperature, which is usually the case for a SG. The observed sharp increase in M with decreasing T indicates the opposite, specifically, that the magnetic clusters increase in size rapidly with decreasing T. The results of the measurements of the initial magnetic susceptibility in an ac magnetic field showed that a sharp maximum is observed on the $\chi(T)$ curves at a temperature T_N, which does not depend on the frequency of the ac magnetic field. As an example, the $\chi(T)$ curves for $Eu_{0.7}Ca_{0.3}MnO_3$ are displayed in Fig. 2. The curves were obtained at different frequencies of the ac magnetic field. It is evident from the figure that T_N does not depend on the indicated frequency. It should be noted that the temperatures T_N and T_f are the same for the composition $EuMnO_3$ (41 K) and are different for the other two compositions, specifically, $T_N = 52$ K and $T_f = 28$ K for $Eu_{0.7}Sr_{0.3}MnO_3$, and $T_N = 65.5$ K and $T_f = 39$ K for $Eu_{0.7}Ca_{0.3}MnO_3$.

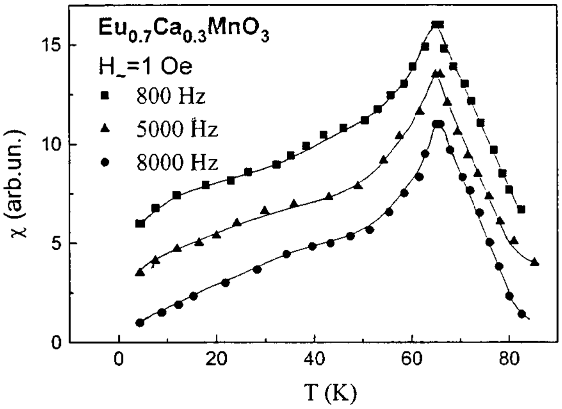

FIG. 2. Temperature dependence of the initial magnetic susceptibility for $Eu_{0.7}Ca_{0.3}MnO_3$ with various frequencies of the ac magnetic field.

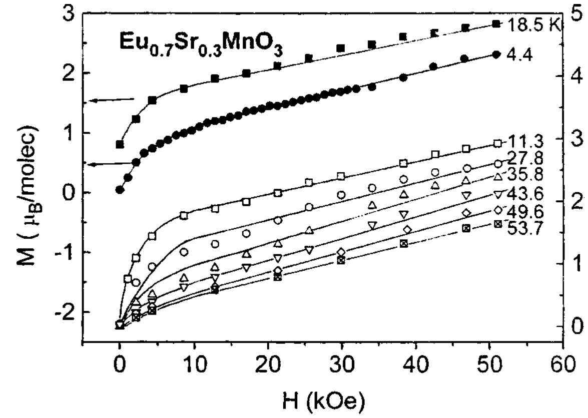

FIG. 3. Magnetization isotherms of $Eu_{0.7}Sr_{0.3}MnO_3$.

Magnetization measurements in high fields, right up to 45 kOe, showed that the $M(H)$ curves obtained after the sample was cooled in a zero field are a superposition of the linear part, characteristic for an antiferromagnet, and a spontaneous magnetization. This is seen clearly in Fig. 3, which shows the magnetization isotherms for $Eu_{0.7}Sr_{0.3}MnO_3$. The following interesting fact is observed under these conditions. As one can see from Fig. 4, a maximum remains on the $M(T)$ curves for $Eu_{0.7}Sr_{0.3}MnO_3$ cooled in a zero field to 4.2 K right up to maximum measurement field 45 kOe, and T_f decreases slightly with increasing field. At the same time, there is no such maximum for the sample cooled in the presence of a nonzero field. The magnetization at the maximum for compositions with Ca and Sr is smaller than the value corresponding to total FM ordering in the sample, specifically, in a 45 kOe field it is 75% of the latter. The temperature dependence of the paramagnetic susceptibility of the compositions $EuMnO_3$, $Eu_{0.7}Ca_{0.3}MnO_3$, and $Eu_{0.7}Sr_{0.3}MnO_3$ follows the Curie–Weiss law. The paramagnetic Curie temperatures θ are -100, 110, and 175 K, respectively.

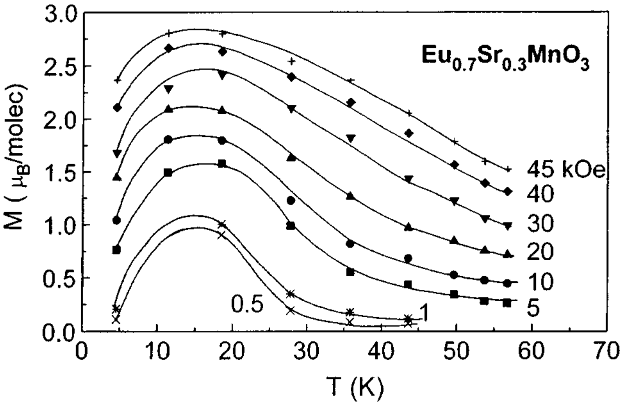

FIG. 4. Temperature dependence of the magnetization of an $Eu_{0.7}Sr_{0.3}MnO_3$ sample in various magnetic fields.

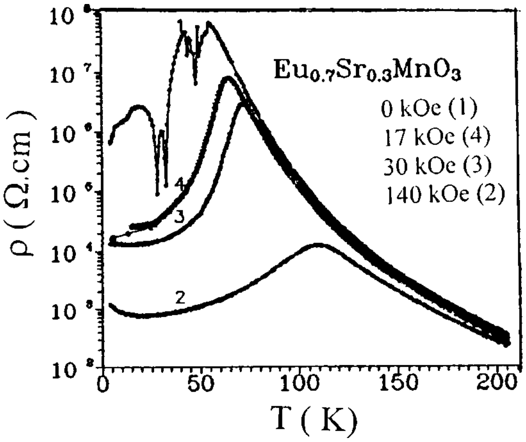

FIG. 5. Temperature dependence of the resistivity of an $Eu_{0.7}Sr_{0.3}MnO_3$ sample in various magnetic fields.

The temperature dependence of the resistivity of $Eu_{0.7}Sr_{0.3}MnO_3$ possesses a maximum near T_N (Fig. 5). The resistivity ρ reaches $10^8\ \Omega\cdot$cm at the maximum. As one can see from Fig. 5, which also shows the effect of an external magnetic field on ρ, under the action of a magnetic field the maximum on the $\rho(T)$ curve decreases and shifts in the direction of higher temperatures. Thus, in a 140 kOe field $\rho_{\max}$ decreased by ~ 4 orders of magnitude, i.e., CMR was observed. However, the temperature dependence $\rho(T)$, measured both in the presence and absence of a magnetic field, at low temperatures is of a semiconductor character and $\rho \geqslant 10^3\ \Omega\cdot$cm. The very large shift of the temperature of $\rho_{\max}$ should also be noted: In a 140 kOe field it is observed at 110 K, which is approximately twice the value of T_N. In $Eu_{0.7}Ca_{0.3}MnO_3$ we also observed a maximum, similar to that shown in Fig. 5, on the $\rho(T)$ curve, but we could not determine the effect of a magnetic field on this curve because of the large fluctuations of the current flowing through the sample. The reason for these fluctuations is unclear to us. In any case, they are not due to the quality of the contacts.

The magnetic and electric properties presented above show that an insulating magnetically two-phase state[1] is present in the compositions studied: In antiferromagnetic (AFM) semiconductors, because of the gain in the $s-d$ exchange energy, charge carriers are localized in FM microregions in an insulating AFM matrix. Such FM droplets exist in at temperatures $T \geqslant 0$ and break down under heating in the region $T \geqslant T_N$. The charge carriers, which at $T < T_N$ are located in FM droplets, become free. This is manifested as a sharp drop in ρ with a further increase of T. For this reason, features are also observed on the $\rho(T)$ curves in this temperature range. In a magnetic field the volume of the FM clusters increases, which facilitates tunneling of charge carriers between clusters. Moreover, a magnetic field orients the magnetic moments of the clusters along the field, which also facilitates tunneling of charge carriers. Finally, a magnetic field increases the kinetic energy of the electrons inside FM clusters and thereby facilitates tunneling of electrons and promotes breakdown of the clusters. This can explain the CMR and the characteristic features in ρ in doped antiferromagnetic $EuMnO_3$ (Fig. 5).

The FM clusters are also the reason that the low-temperature magnetic properties depend on the thermomagnetic history of the sample (Fig. 1). The rapid growth of the magnetization with decreasing temperature of a sample cooled in a nonzero field indicates that the FM clusters increase in size, which is also characteristic for an insulating magnetically two-phase state. This fact cannot be explained on the basis of spin-glass and superparamagnetism models, in which the indicated magnetization is essentially temperature-independent below T_f (Ref. 9). The displacement of the hysteresis loop of a sample cooled in a nonzero field should be specially noted (inset in Fig. 1). Such shifted hysteresis loops have been observed by Meiklejohn and Bean in partially oxidized Co and were attributed to an exchange interaction between the FM Co particles and the AFM CoO particles.[10] At high temperatures the magnetic anisotropy of the AFM part of the sample is low, and the AFM vector orients the magnetic moments of the Co particles along its direction. On cooling to low temperatures the magnetic anisotropy of the AFM part of the sample increases rapidly and very high, oppositely directed fields are required to reverse the magnetization of the AFM part of the sample. However, when the magnetic field applied in a direction opposite to the magnetization of the sample is strong enough to break the exchange coupling of the FM and AFM parts of the sample, the magnetization of the FM part of the sample is reversed but the AFM vector is not reversed. As the field decreases, the magnetization of the sample abruptly changes direction and becomes oriented in a direction opposite to the field, and it reaches its previous value. This happens when the energy of the magnetic field becomes less than the exchange energy of the FM and AFM parts of the sample. At the present time, the hysteresis loops described above are considered to be one of the proofs for an SG state in the material.[9] At the same time, this phenomenon can be explained only for cluster SGs and cannot be explained for an ideal SG consisting of individual spins. Kouvel attempted to explain, just as described above, the displaced hysteresis loops that he observed in the SGs CuMn and AgMn.[11] He was forced to assume that the distribution of Mn atoms in the sample is nonuniform in these materials: He assumed the Mn-depleted regions to be FM and the Mn-enriched regions AFM. In light of this, the displaced hysteresis loops should be one of the indications of an insulating magnetically two-phase state, as was observed in the present work.

Apparently, the sharp maximum which is measured in the temperature dependence of χ in an ac magnetic field and which does not depend on the frequency of this field (Fig. 2) indicates AFM ordering in the main matrix. The temperature of the indicated maximum in this case is the Néel temperature. This temperature cannot be the freezing temperature of the SG, since the latter ordinarily depends on the measurement frequency.[9] The maximum in the $M(T)$ curves, which were obtained after the sample was cooled in a zero field (Figs. 1 and 4), at $T=T_f$ likewise attests to the presence of FM clusters in the sample. The temperature T_f corresponds to the blocking temperature of these clusters, if they do not interact with one another (analog of superparamagnetism), or the freezing temperature, if an interaction exists between them (analog of a cluster SG). In both cases this temperature should decrease with increasing magnetic field,[9] as we observed (Fig. 4). The fact that, as one can see from Fig. 3, the magnetization isotherms are a superposition of a linear part, characteristic for an antiferromagnet, and a small spontaneous part, which can easily originate from FM droplets, also indicates a magnetically two-phase state. The rapid increase of θ in compositions with Ca and Sr as compared with θ for $EuMnO_3$ attests to a large contribution of FM exchange to the total exchange in the sample, which, probably occurs from FM clusters. As indicated above, the temperature at which the FM droplets are destroyed is close to T_N,[1] and an external magnetic field increases the temperature at which this occurs. This is due to the fact that a magnetic field is intensified near impurities by $s-d$ exchange and thereby impedes thermal destruction of FM droplets.[1] Indeed, the transition into a paramagnetic state on the $M(T)$ curves (Fig. 4) strongly depends on the magnitude of the magnetic field in which it occurs: In the field $H=0.5$ kOe at $T\sim 30$ K, and in the field $H=45$ kOe the transition is strongly broadened and is still not complete at $T=55$ K. As a result of this, the maximum on the $\rho(T)$ curves shifts in the direction of higher temperatures (Fig. 5).

This work was supported by the Russian Fund for Fundamental Research, Project No. 96-15-96429. We are grateful to Ya. M. Mukovskiĭ for preparing and analyzing the samples and for measuring the temperature dependence of the resistivity.

*e-mail: koroleva@ofef343.phys.msu.su

---

[1] É. L. Nagaev, Usp. Fiz. Nauk **166**, 833 (1996).
[2] A. P. Ramirez, J. Phys.: Condens. Matter **9**, 8171 (1997).
[3] R. Pauthenet and C. Veyret, J. Phys. (Paris) **31**, 65 (1970).
[4] I. O. Troyanchuk, H. Szymczak, N. V. Samsonenko, and A. Nabialek, Phys. Status Solidi A **157**, 167 (1996).
[5] I. O. Troyanchuk, N. V. Samsonenko, G. Shimchak, and F. Nabyalek, Fiz. Tverd. Tela (St. Petersburg) **39**, 117 (1997) [Phys. Solid State **39**, 101 (1997)].
[6] I. O. Troyanchuk, F. V. Zubets, and E. F. Shapovalova, Izv. Akad. Nauk SSSR Neorg. Mater. **33**, 1512 (1997).
[7] A. Sundaresan, A. Maignan, and B. Raveau, Phys. Rev. B **55**, 5596 (1997).
[8] Y. M. Mukovski, G. Hischer, H. Michor, and A. M. Ionov, J. Appl. Phys. **83**, 7163 (1998).
[9] K. H. Fischer, Phys. Status Solidi B **116**, 357 (1983).
[10] W. H. Meiklejohn and C. P. Bean, Phys. Rev. **102**, 1413 (1956); **105**, 904 (1957).
[11] J. S. Kouvel, J. Phys. Chem. Solids **21**, 57 (1961); **24**, 795 (1963).

Translated by M. E. Alferieff

JETP LETTERS VOLUME 69, NUMBER 5 10 MARCH 1999

Role of the curvature of atomic layers in electron field emission from graphitic nanostructured carbon

A. N. Obraztsov, A. P. Volkov, and I. Yu. Pavlovskiĭ
M. V. Lomonosov Moscow State University, 119899 Moscow, Russia

A. L. Chuvilin, N. A. Rudina, and V. L. Kuznetsov
G. K. Boreskov Institute of Catalysis, Russian Academy of Sciences, 630090 Novosibirsk, Russia

(Submitted 3 February 1999)
Pis'ma Zh. Éksp. Teor. Fiz. **69**, No. 5, 381–386 (10 March 1999)

Layers of oriented carbon nanotubes and nanometer-size plate-shaped graphite crystallites are obtained by chemical vapor deposition in a glow-discharge plasma. A structural–morphological investigation of a carbon material consisting of nanotubes and nanocrystallites is performed, and the field-emission properties of the material are also investigated. It is shown that electron field emission is observed in an electric field with average intensity equal to or greater than 1.5 V/μm. The low fields giving rise to electron emission can be explained by a decrease in the electronic work function as a result of the curvature of the atomic layers of graphitic carbon. © *1999 American Institute of Physics.* [S0021-3640(99)00905-6]

PACS numbers: 79.70.+q, 73.61.Tm, 81.15.Gh, 36.40.−c

Carbon is well known for its capability of existing in various polymorphic modifications (diamond, graphite, carbyne) differing by the type of interatomic bonds.[1] Another remarkable feature of carbon is that nanometer-size clusters distinguished by a remarkable diversity of geometric forms can be formed by atoms bound with one another predominantly by a graphitic type bond.[2] Such nanostructured clusters include, specifically, fullerenes and carbon nanotubes, which have become well-known in recent years because of a variety of unique properties. One such property manifested by carbon nanotubes is the extremely low electric field (E) in which electron field emission is observed experimentally.[3–6] For nanotubes this value is more than four orders of magnitude lower than the fields $E=10^6-10^7$ V/cm in which electron field emission is observed in typical metals and semiconductors.[7]

Ordinarily, such a large decrease of the average field intensity E is explained by a local enhancement of the field on the surfaces of tips, such as individual nanotubes. A simple estimate shows that the emitting region does not exceed fractions of a nanometer in size, which is much smaller than the minimum diameter of nanotubes (about 1 nm). Various models taking account of, to one degree or another, the possibility that the emitting region decreases in size and the emitter length increases, are proposed to explain this contradiction. A typical example is Ref. 4, where it is supposed that chains of carbon atoms can form at the end of an emitting carbon nanotube. The authors suppose that last atom in the chain is the source of the field-emitted electrons. The emission current density is found to be higher than the maximum possible density for field emission $10^{10}-10^{11}$ A/cm^2, above which explosive breakdown of the emitter is observed even at values only slightly higher than the limit.[8]

In the present letter an alternative explanation of the decrease in the field intensity required for electron field emission from carbon nanotubes and other clusters of graphitic carbon is proposed on the basis of an analysis of the experimental data obtained by investigating the field emission from carbon films deposited using a novel method.

EXPERIMENTAL CONDITIONS

The experimental samples of carbon films were obtained by chemical vapor deposition of carbon from a dc-discharge-activated mixture of methane and hydrogen. The equipment used for this is described in detail in Ref. 9. The films were deposited on a 25×25 mm KÉF 4.5 (100) silicon substrate. The methane concentration was about 10% and the substrate temperature was about 1050 °C.

The phase composition of the films obtained was investigated using Raman scattering (RS) spectroscopy and electron diffraction. The structural–morphological features of the films were analyzed using a JEM-4000EX high-resolution transmission electron microscope. To obtain an image of the structure of the near-surface layers of the carbon films with high resolution, samples were prepared in the form of wedge-shaped chips of the silicon substrate with the film. When such a sample was arranged so that the axis of the electron beam of the microscope was parallel to the substrate plane, the film fragments remaining on the sharp tip were thin enough so that an image of their structure could be obtained ‘‘in transmission.’’

The investigation of field emission consisted in measuring the current–voltage characteristics (IVCs) of the emitter in the vacuum-diode regime. The minimum detected current of emitted electrons was several picoamperes. The measurements were performed in an approximately 10^{-6} torr vacuum. To determine the density distribution of the emitting centers over the surface of the film, we used an anode in the form of a glass plate with an electrically conducting transparent layer of tin oxide on which a cathodoluminophor had been deposited.

RESULTS AND DISCUSSION

Two lines were observed in the RS spectra of the experimental carbon films — a relatively intense and narrow line at about 1580 cm^{-1} and a much weaker line at about 1350 cm^{-1}. Such spectra are characteristic for various graphitic materials, including polycrystalline graphite itself[10] or, for example, multiwall carbon tubes.[11,12] These RS-spectroscopy data, already discussed in our recent publications, just as the results of electron diffraction investigations,[13,14] make it possible to conclude only that the films obtained consist of nanometer-size clusters of graphitic carbon.

More complete information about the structural features of the carbon films prepared using the method described above was obtained with a high-resolution electron microscope. Figure 1a shows a typical image, obtained using a transmission electron microscope, of a near-surface layer of the film. It is evident from this image that needle-shaped

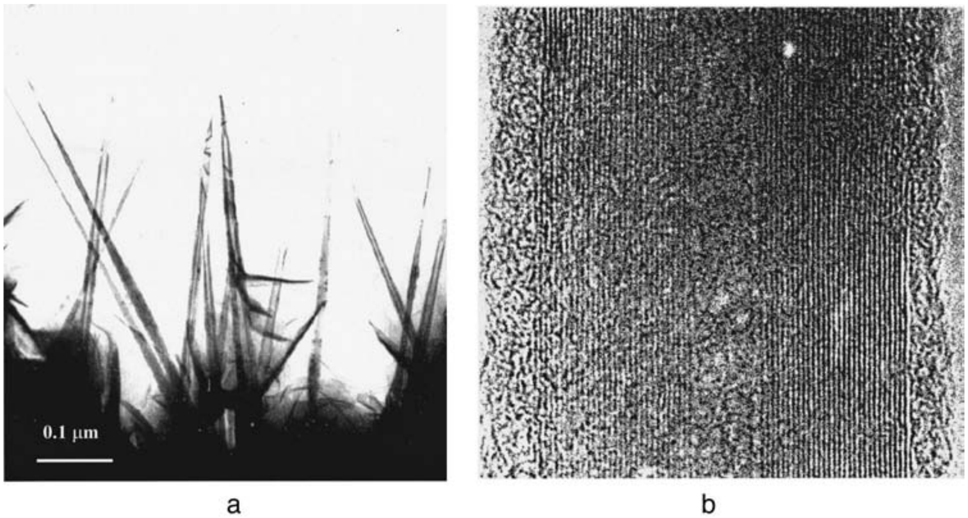

FIG. 1. Electron micrograph of a section of the film surface consisting of oriented carbon nanotubes (a) and a micrograph, obtained with large magnification, of a fragment of one nanotube (b).

formations, ranging in diameter at the base from several to hundreds of nanometers and up to several microns long, oriented predominantly perpendicular to the substrate are present on the film surface. An enlarged image of a fragment of one such formation is shown in Fig. 1b, from which it follows that this fragment consists of several coaxial cylindrical layers of atoms with an interlayer distance of about 0.34 nm, equal to the interplanar distance in crystalline graphite and carbon nanotubes.

It is also evident from Fig. 1a that, besides carbon nanotubes, the surface of the film contains a large number of plate-shaped formations, which electron diffraction investigations[13,14] show to be graphite crystallites several nanometers thick. In some cases such platelike crystallites form structures similar to the one shown in Fig. 2. A characteristic feature of these crystallites is the presence of a large number of sections with a curved surface.

The results of the investigation of electron field emission from the carbon films examined above are presented in Fig. 3 in the form of an IVC for a vacuum diode in which the cathode consisted of a carbon film on a silicon substrate and the anode consisted of a 20 mm in diameter tungsten disk. The cathode–anode distance was 150 μm. The IVC presented in Fig. 3 is plotted in Fowler–Nordheim coordinates, and its linear character reflects the correspondence between the observed curve and the well-known relation for electron field emission (see, for example, Refs. 4 and 7)

$$I = A(\beta V)^2 \exp(-B\varphi^{3/2}/\beta V), \tag{1}$$

where $A = 1.4\times 10^{-2}$ and $B = 6.8\times 10^9$ for current density I in A/m^2 and effective energy barrier for electrons at the emitter–vacuum boundary (effective work function) φ in electron volts; V is the voltage (in volts) applied between the anode and the cathode. The quantity β is given by $\beta = \beta^* d$, where d is the anode–cathode distance in meters and β^* characterizes the local enhancement of the electric field because of the geometric form of

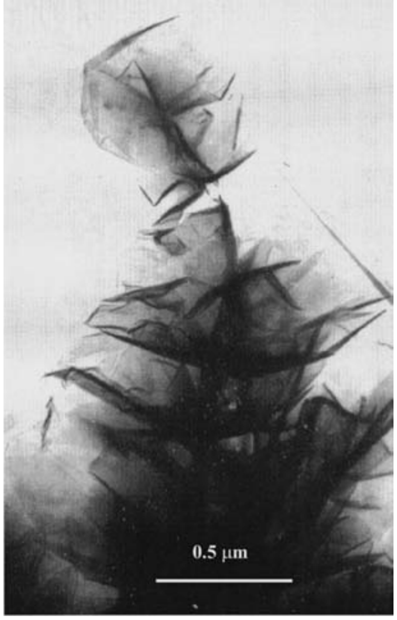

FIG. 2. Electron micrograph of a section of the film surface consisting of plate-shaped graphite nanocrystallites.

the emitter surface. For a flat cathode $\beta^* = 1$, while for a cathode in the form of a tip of height h and radius of curvature r at the end, to a good approximation, $\beta^* = h/r$ (Ref. 4).

Using the electron micrographs (see Fig. 1), we estimated the geometric field enhancement factor for nanotubes as $100 < \beta^* < 1000$. Substituting this value into Eq. (1) makes it possible to estimate from the slope of the IVC in Fig. 3 the effective work function φ, which is found to be in the range 0.5–2 eV, which is much lower than the characteristic value for graphite, which is 5 eV.[5,15] As we have pointed out previously,[13] the decrease in the work function could be due to a modification of the electronic configuration of the carbon atoms located at the edge of the atomic layer in graphitic clusters. However, the results presented above, obtained with a high-resolution electron microscope, show that the presence of bends in the atomic layers in such clusters could be more important.

For atoms located near a bend in a layer, the electronic configuration should also be modified as a result of a change in the degree of overlap of the $p\pi$ electronic orbitals oriented perpendicular to the plane of the layer. This is shown schematically in Fig. 4a. Moreover, thermodynamic considerations[16] show that the presence of an atomic layer of carbon atoms with dangling bonds at the edge[13] is less favorable than the formation of arc-shaped structures closing the edges of the parallel layers of graphitic carbon (Fig. 4b). We observed a similar behavior of graphitic carbon in an investigation of the graphitization of polycrystalline diamond.[17]

The change in the degree of overlap of $p\pi$ electronic orbitals of atoms near a bend can be accompanied by a change in the type of hybridization of electronic bonds from graphitic (sp^2) to diamondlike (sp^3).[16] The spectrum of the electronic states of such

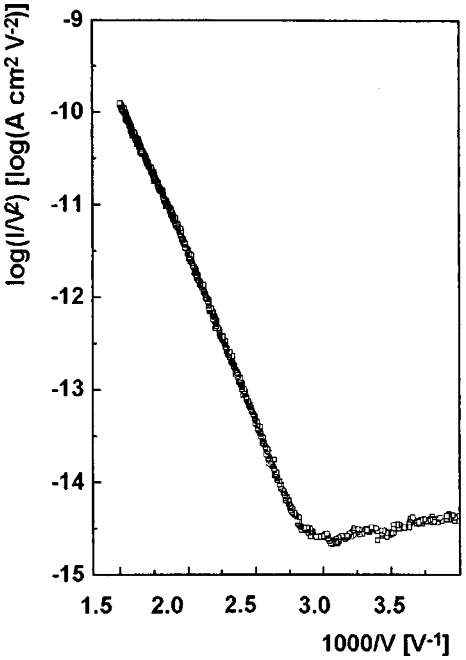

FIG. 3. Typical current–voltage characteristic in Fowler–Nordheim coordinates for a vacuum diode with a carbon-film field-emission cathode.

carbon atoms will be determined by π electrons similarly to the manner in which this occurs in another carbon material — diamond. The degree of delocalization of the corresponding energy levels can be quite high because atoms whose electronic configuration is modified as a result of an bend form macroscopically large regions on the surfaces of clusters. The electronic properties of these atoms have a greater similarity to diamond than graphite. Specifically, their spectrum of electronic states should contain levels sepa-

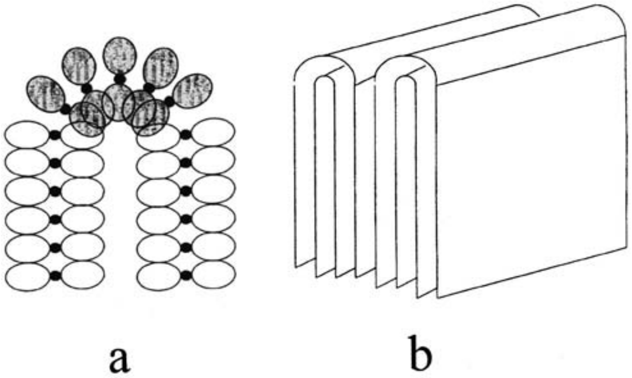

FIG. 4. Schematic representation of a bent layer of carbon atoms (a) and bent layers at the edges of graphite crystallites (b).

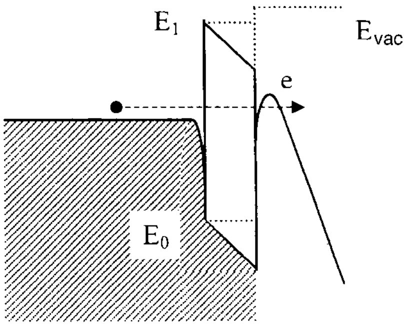

FIG. 5. Energy band diagram for a near-surface region of a film of graphitic material.

rated by an energy gap close in width to the band gap in diamond (5.5 eV), as shown in the band diagram in Fig. 5. Just as in diamond (or other wide-gap materials), the ‘‘conduction-band’’ bottom (the level E_1 in Fig. 5) of the modified carbon material near a bend can be expected to lie quite close to the electron level in vacuum (E_{vac}). It is obvious that the thickness of a layer of such atoms, which is equal to 1–2 interplanar distances in graphite (0.34 nm), is tunneling transparent to electrons, which will be injected into the ‘‘conduction band’’ under the action of a corresponding electric field. The barrier height for electrons emitted into vacuum ($E_{\mathrm{vac}}-E_1$; see Fig. 5) will be much lower than for graphite.

The foregoing considerations are all applicable not only to the region of a bend in the atomic layers at the edges of graphitic clusters but also for bends formed in a different manner, for example, as a result of the formation of nanotubes or folds on the surface of plate-shaped nanocrystallites (see Figs. 1 and 2). The radius of curvature of these regions for which the above-described decrease of the energy barrier for emitted electrons can be observed can vary wide limits. The total area of such regions on the surface of carbon films can be quite large, but only the electrons that are located on the clusters protruding above the film surface will participate in electron field emission.

In summary, the large decrease in the electric field required for field emission from films of nanostructured graphitic carbon could be due to the combined effect of two factors: (i) a local enhancement of the electric field on the geometric features of the films, consisting of nanostructured graphitic carbon, and (ii) a decrease of the effective height of the energy barrier for electrons escaping from the film surface near a bend in the corresponding atomic layers.

This work was supported in part by the Federal Target Program ‘‘Integratsiya’’ (Project No. K1129) and by INTAS (Grant No. 1997–1700).

[1] L. I. Man, Yu. A. Malinovskiĭ, and S. A. Semiletov, Kristallografiya **35**, 1029 (1990) [Sov. Phys. Crystallogr. **35**, 608 (1990)].
[2] M. Terrones, W. K. Hsu, J. P. Hare *et al.*, Philos. Trans. R. Soc. London, Ser. A **354**, 2025 (1996).
[3] Z. Ya. Kosakovskaya, L. A. Chernozatonskiĭ, and E. A. Fedorov, JETP Lett. **56**, 26 (1992).
[4] A. G. Rinzler, J. H. Hafner, P. Nikolaev *et al.*, Science **269**, 1550 (1995).
[5] W. A. de Heer, A. Châtelain, and D. Ugarte, Science **270**, 1179 (1995).
[6] Y. Saito, K. Hamaguchi, K. Hata *et al.*, Nature (London) **389**, 555 (1997).
[7] M. I. Elinson (Ed.), *Cold Cathodes* [in Russian], Sov. Radio, Moscow, 1974.

[8] G. N. Furseĭ, D. V. Glazanov, L. M. Baskin *et al.*, Mikroelektronika **26**, 89 (1997).
[9] I. Yu. Pavlovskiĭ and A. N. Obraztsov, Prib. Tekh. Éksp. No. 1, 152 (1998).
[10] R. E. Shroder, R. J. Nemanich, and J. T. Glass, Phys. Rev. B **41**, 3738 (1990).
[11] J. M. Holden, P. Zhou, X.-X. Bi *et al.*, Chin. Phys. Lasers **220**, 186 (1994).
[12] N. V. Khokhryakov, S. S. Savinskiĭ, and J. M. Molina, JETP Lett. **62**, 617 (1995).
[13] A. N. Obraztsov, A. P. Volkov, and I. Yu. Pavlovskiĭ, JETP Lett. **68**, 59 (1998).
[14] A. N. Obraztsov, I. Yu. Pavlovsky, A. P. Volkov *et al.*, in *Proceedings of the 9th European Conference DIAMOND'98*, Abstract No. 15.514 (full paper accepted for publication in Diamond Related Mater.).
[15] J.-M. Bonard, T. Stöckli, F. Maier *et al.*, Phys. Rev. Lett. **81**, 1441 (1998).
[16] H. Hiura, T. W. Ebbeesen, J. Fujita *et al.*, Nature (London) **367**, 148 (1994).
[17] V. L. Kuznetsov, A. L. Chuvilin, Yu. V. Butenko *et al.*, Chem. Phys. Lett. **289**, 353 (1998).

Translated by M. E. Alferieff

JETP LETTERS VOLUME 69, NUMBER 5 10 MARCH 1999

Weak collapse in the nonlinear Schrödinger equation

Yu. N. Ovchinnikov
L. D. Landau Intitute of Theoretical Physics, Russian Academy of Sciences,
117940 Moscow, Russia

(Submitted 28 January 1999)
Pis'ma Zh. Éksp. Teor. Fiz. **69**, No. 5, 387–390 (10 March 1999)

It is shown that there exists a three-parameter family of exact solutions of the nonlinear Schrödinger equation that lead to weak collapse. © *1999 American Institute of Physics.* [S0021-3640(99)01005-1]

PACS numbers: 03.65.Ge, 02.30.Jr

The nonlinear Schrödinger equation

$$i\frac{\partial\psi}{\partial t}+\Delta\psi+|\psi|^{2\sigma}\psi=0, \tag{1}$$

where ψ is a scalar function in d-dimensional space and Δ is the Laplacian operator, arises in a number of physical problems. Such an equation has been obtained in plasma physics and nonlinear optics.[1–3] The nonlinear term in Eq. (1) corresponds to attraction. As a result, for any $\sigma>0$ the uniform state $\psi=a\exp(ia^{2\sigma}t)$ is unstable with respect to infinitesimal disturbances. The dispersion relation is $\omega^2=K^2(K^2-2\sigma a^{2\sigma})$, $\psi=(a+\delta\psi)\exp(ia^2t)$. Solutions of Eq. (1) that have a singular point at a finite time t_0 exist for $\sigma d>2$.

Equation (1) conserves the total number of particles and the total energy. The energy E_V and the number of particles N_V in a volume V are given by the expressions

$$E_V=\frac{1}{2}\int_V d^d r\left\{|\nabla\psi|^2-\frac{1}{1+\sigma}|\psi|^{2(1+\sigma)}\right\},\quad N_V=\int_V d^d\mathbf{r}|\psi|^2,\quad \nabla\equiv\text{grad}. \tag{2}$$

The equations (1) and (2) determine the following expression for the particle flux density j_n and the energy flux density j_E:

$$j_n=i(\psi\nabla\psi^*-\psi^*\nabla\psi),\quad j_E=-\frac{1}{2}\left(\nabla\psi^*\frac{\partial\psi}{\partial t}+\frac{\partial\psi^*}{\partial t}\nabla\psi\right). \tag{3}$$

We shall seek the collapsing solutions of Eq. (1) in a spherically symmetric form

$$\psi(\mathbf{r},t)=\lambda^{\nu}\varphi(\rho\lambda)\exp(i\chi(\rho,t)), \tag{4}$$

where $\lambda\equiv\lambda(t)$, φ is a real function, and ν is a numerical parameter.

The condition that the total particle flux through a spherical surface of radius ρ equals the change in the particle number N_V inside a sphere gives an equation for the phase χ:

$$-2\frac{\partial\chi(\rho,t)}{\partial\rho}=\frac{\rho}{\lambda}\frac{\partial\lambda}{\partial t}+\frac{2\nu-d}{\varphi^2(y)}\frac{1}{y^{d-1}}\frac{1}{\lambda^2}\frac{\partial\lambda}{\partial t}\int_0^y dy\,y^{d-1}\varphi^2(y), \tag{5}$$

where $y=\rho\lambda$. We find from Eqs. (2), (3), and (4)

$$E_V=\frac{\alpha}{2}\int_0^\rho d\rho\,\rho^{d-1}\left\{\varphi^2\lambda^{2\nu}\left(\frac{\partial\chi}{\partial\rho}\right)^2+\lambda^{2\nu+2}(\varphi')^2-\frac{\lambda^{2\nu(1+\sigma)}}{1+\sigma}\varphi^{2(1+\sigma)}\right\},$$

$$\frac{\partial E_V}{\partial t}=\alpha\lambda^{2\nu}\rho^{d-1}\left\{(\nu\varphi+y\varphi')\varphi'\frac{\partial\lambda}{\partial t}+\frac{\partial\chi}{\partial t}\frac{\partial\chi}{\partial\rho}\varphi^2\right\}. \tag{6}$$

The prime in Eqs. (6) denotes the derivative $\partial/\partial y$, $\alpha=2\pi^{d/2}/\Gamma(d/2)$ is the coefficient in the expression for the ‘‘area’’ of a spherical surface $S(\rho)=\alpha\rho^{d-1}$, and $\Gamma(x)$ is Euler's gamma function. In order that all terms in Eqs. (5) and (6) have the same time dependence for $\nu\neq d/2$ the following conditions must be satisfied:

$$\nu\sigma=1,\quad \chi(\rho,t)=\chi_0(t)+\tilde{\chi}(\rho\lambda),$$

$$\frac{1}{\lambda^3}\frac{\partial\lambda}{\partial t}=\text{const};\quad \frac{\partial\chi_0}{\partial t}\sim\frac{1}{\lambda}\frac{\partial\lambda}{\partial t}. \tag{7}$$

From Eqs. (7) we find

$$\lambda=\frac{C}{\sqrt{t_0-t}},\quad \chi_0(t)=-\frac{C_1}{2}\ln(t_0-t),\quad \frac{1}{\lambda^3}\frac{\partial\lambda}{\partial t}=\frac{1}{2C^2},\quad \frac{\partial\chi_0}{\partial t}=\frac{C_1\lambda^2}{2C^2}, \tag{8}$$

where C, C_1, and t_0 are constants.

Let us now consider the physically more interesting case $d=3$, $\sigma=1$. The general case of arbitrary values of $\{d,\sigma\}$ will be considered separately. Substituting expressions (8), Eq. (6) for the phase $\tilde{\chi}$ assumes the form

$$\tilde{\chi}'+\frac{1}{4C^2}\left(y-\frac{1}{y^2\varphi^2}\int_0^y dy\,y^2\varphi^2\right)=0. \tag{9}$$

The modulus φ satisfies the equation

$$\frac{1}{y^2}\frac{\partial}{\partial y}\left(y^2\frac{\partial\varphi}{\partial y}\right)+\varphi^3-\frac{\varphi}{2C^2}(C_1+y\tilde{\chi}')-\varphi(\tilde{\chi}')^2=0. \tag{10}$$

We note that any solution of the system of equations (9) and (10) is an exact solution of the nonlinear equation (1). Let

$$Z=\int_0^y dy\,y^2\varphi^2. \tag{11}$$

A simple relation between the function Z and the functions φ and $\tilde{\chi}$ follows from Eqs. (9) and (11):

$$\varphi=\frac{\sqrt{Z'}}{y},\quad \tilde{\chi}'=-\frac{yZ'-Z}{4C^2Z'},\quad \tilde{\chi}(y)=\text{const}-\frac{1}{4C^2}\int_0^y dy\frac{yZ'-Z}{Z'}. \tag{12}$$

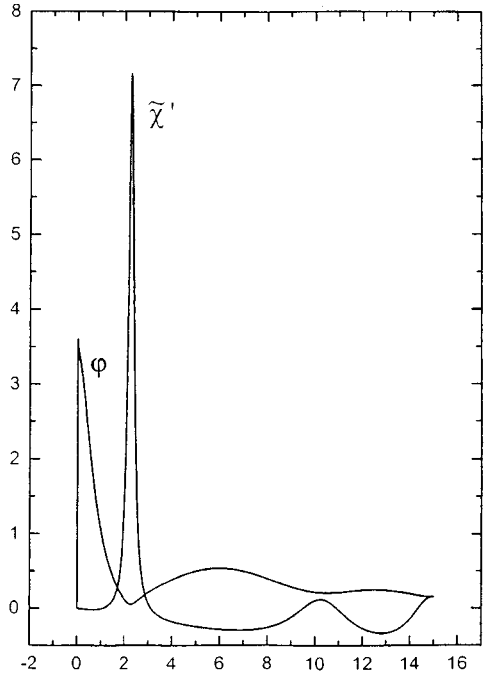

FIG. 1. The functions φ and $\tilde{\chi}'$ for the parameters $\{A,C,C_1\}=\{4,2,2\}$.

Substituting the expressions for φ and $\tilde{\chi}$ from Eq. (12) into Eq. (10) we obtain a single ordinary differential equation for the function Z:

$$Z''' - \frac{(Z'')^2}{2Z'} + \frac{2(Z')^2}{y^2} - \frac{1}{C^2}\left(C_1 Z' - \frac{y}{4C^2}(yZ'-Z) \right) - \frac{(yZ'-Z)^2}{8C^4 Z'} = 0. \tag{13}$$

In the region $y \ll 1$ we obtain from Eq. (13)

$$Z(y) = Ay^3 + \frac{y^5}{15}\left(\frac{3AC_1}{2C^2} - 9A^2 \right) + \dots, \tag{14}$$

where $A>0$ is an arbitrary constant. In the region $y \gg 1$ the asymptotic solution of Eq. (13) is

$$Z = By - \frac{2BC^2C_1}{y} + \frac{2BC^4}{y^3}(B - 2C_1^2) + \dots \tag{15}$$

The equation (13) admits the existence of poles of the form

$$Z = -\frac{2y_0^2}{y_0 - y}. \tag{16}$$

However, for $A>0$ it is impossible to reach such a pole. It also follows from Eq. (13) that the function Z' does not vanish for $y>0$. Since in the limit $y \to \infty$ the only possible

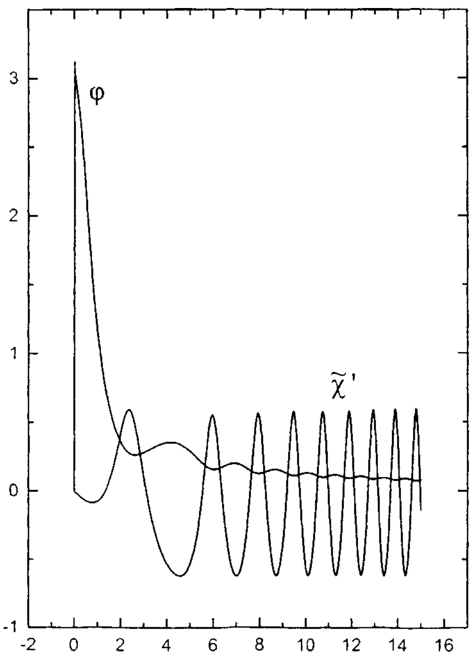

FIG. 2. The functions φ and $\tilde{\chi}'$ for the parameters $\{A,C,C_1\}=\{3,1,1\}$.

asymptotic solution of Eq. (13) is determined (for $A>0$) by Eq. (14), there exists a three-parameter family of functions $\varphi(y)$ that give a solution of Eq. (1). These parameters are $\{A,C,C_1\}$.

The region of physical collapse is always bounded. Let

$$\tilde{\varphi}(\rho)=\begin{cases}\varphi(\rho) & \text{for } y<y^*,\\ 0 & \text{for } y>y^*.\end{cases} \tag{17}$$

The point y^* must be chosen so that

$$\varphi(0)\gg\varphi(y^*). \tag{18}$$

For the appropriate choice of the parameters $\{A,C,C_1\}$ the condition (18) can be satisfied even if $y^*\lesssim 1$. The function $\varphi(y)$ for this choice of the parameters $\{A,C,C_1\}$ possesses a deep minimum, whose position must be taken as the point y^*. Cutting the solution off at the point y^*will lead to the appearance of a weak outgoing wave $\psi_1(\rho,t)$, whose smallness is determined by the inequality (18). Figures 1 and 2 show the values of functions $\varphi(y)$ and $\tilde{\chi}(y)$ for two sets of parameters: $\{A,C,C_1\}=\{4,2,2\}$ — Fig. 1 and $\{A,C,C_1\}=\{3,1,1\}$ — Fig. 2. The ratio $\varphi(0)/\varphi(y^*)$ for the parameters in Fig. 1 is $\varphi(0)/\varphi(y^*)=71.3$ and $y^*=2.26$.

The collapsing solution of Eq. (1) is given by the expression

$$\psi(\mathbf{r},t)=\lambda\tilde{\varphi}(\rho\lambda)\exp\left\{-\frac{iC_1}{2}\ln(t_0-t)+i\tilde{\chi}(\rho\lambda)\right\}+\psi_1(\rho,t), \tag{19}$$

where the function $\psi_1(\rho,t)$ is the solution of the linear equation

$$i\frac{\partial\psi_1}{\partial t}+\Delta\psi_1+2|\psi|^2\psi_1+\psi^2\psi_1-\frac{iy^*\varphi(y^*)}{2(t_0-t)}\delta\left(\rho-\frac{y^*}{\lambda}\right)e^{i\chi(\rho,t)}$$

$$-\frac{\lambda\varphi(y^*)}{\rho^2}\frac{\partial}{\partial\rho}\left(\rho^2\delta\left(\rho-\frac{y^*}{\lambda}\right)e^{i\chi(\rho,t)}\right)=0 \qquad (20)$$

with the initial condition $\psi_1(\rho^*,t)=0$, where t^* is the moment at which collapse starts.

Investigation of the stability of the solution (19) and the conditions under which the function $\psi_1(\rho,t)$ remains a small correction to expressions (4) and (19) falls outside the scope of this letter. Weak collapse has been studied in Refs. 4 and 5.

A collapsing solution arises in a bounded region of space, and an initial distribution of a special form must be produced in order for a singularity to arise. In numerical simulation or in real physical objects, collapse will arise from fluctuations that lead to collapse and which appear with a probability close to the maximum value.

I thank S. P. Novikov, A. B. Shabat, and E. A. Kuznetsov for a discussion of the results and for valuable remarks.

Yu. N. Ovchinnikov's work is supported by Grant CRDF RP1-194.

[1] V. E. Zakharov, Zh. Éksp. Teor. Fiz. **62**, 1746 (1972) [Sov. Phys. JETP **35**, 908 (1972)].
[2] V. E. Zakharov and V. S. Synakh, Zh. Éksp. Teor. Fiz. **68**, 940 (1975) [Sov. Phys. JETP **41**, 464 (1976)].
[3] A. Dyachenko, A. C. Newell, A. Pushkarev, and V. E. Zakharov, Physica D **57**, 96 (1992).
[4] V. E. Zakharov and L. N. Shur, Zh. Éksp. Teor. Fiz. **81**, 2019 (1981) [Sov. Phys. JETP **54**, 1064 (1981)].
[5] V. E. Zakharov and E. A. Kuznetsov, Zh. Éksp. Teor. Fiz. **91**, 1310 (1986) [Sov. Phys. JETP **64**, 773 (1986)].

Translated by M. E. Alferieff

JETP LETTERS VOLUME 69, NUMBER 5 10 MARCH 1999

Hierarchical representation of generalized (nonadditive) thermodynamics

A. I. Olemskoĭ*
Sumy State University, 244007 Sumy, Ukraine

(Submitted 28 January 1999)
Pis'ma Zh. Éksp. Teor. Fiz. **69**, No. 5, 391–394 (10 March 1999)

A recurrence relation leading to a probability distribution of microstates at different hierarchical levels of a nonadditive statistical system is examined (for the upper level the relation reduces to the Tsallis distribution [C. Tsallis, Physica A **221**, 227 (1995)]). The processes leading to the formation and decay of a hierarchical statistical ensemble are described.
[S0021-3640(99)01105-6]

PACS numbers: 05.70.−a, 05.20.−y

The generalized Gibbs distribution

$$P_q(\epsilon) \propto [1-(1-q)\beta\varepsilon]^{1/(1-q)}, \tag{1}$$

which reduces to the ordinary exponential form in the limit $q \to 1$ (β is the reciprocal of the temperature and ε is the microstate energy), has been under wide discussion in recent years (see Ref. 1 and the references cited therein). This distribution is obtained by the standard variational procedure for the generalized entropy

$$S_q = (q-1)^{-1}\left(1 - \sum_\varepsilon P^q(\varepsilon)\right)$$

under the conditions

$$\sum_\varepsilon P(\varepsilon) = 1, \quad \langle\varepsilon\rangle_q \equiv \sum_\varepsilon \varepsilon P^q(\varepsilon) = \text{const.}$$

A generalization of this kind is used in Ref. 2 to construct a theory of multifractal sets. According to Ref. 3, the distribution (1) corresponds to scale-invariant statistical systems whose phase space exhibits a fractal structure, and the corresponding statistical ensemble is hierarchically subordinated. We shall consider below a modified Fokker–Planck equation, whose solution leads to a distribution over hierarchical levels, on the topmost level of which the relation (1) obtains.

For self-similar systems the number N_k of nodes at the level $k = 1,2,\dots,k_m$ of a hierarchical tree can be represented by a power law $N_k = k^a$, $0 < a < 1$ (see Ref. 4). The function $U(P) = \varepsilon P^q$, with $\varepsilon > 0$ and $0 < q < 1$, will give the coupling between the neighboring levels. The recurrence relation[5]

$$P_{k-1}=P_k+N_k^{-1}U(P_k) \tag{2}$$

relates probabilities P_k of the realization of states at different hierarchical levels k. In the continuum approximation ($1\ll k\ll k_m$) the solution is

$$P_k\propto\left(1-\frac{1-q}{1-a}\varepsilon k^{1-a}\right)^{1/(1-q)}. \tag{3}$$

For a complete ensemble corresponding to the upper level $k=1$, the distribution (3) reduces to the distribution (1) if $\varepsilon\equiv(1-a)\beta\varepsilon$. As k increases, the probability P_k, as expected, decreases. The moments of the distribution (3)

$$\langle k^n\rangle_q\equiv\int_1^{k_m}k^nP_k^q dk, \quad n=1,2,\ldots$$

have the form

$$\langle k^n\rangle_q=A((1-q)\beta\varepsilon)^{-n/(1-a)}\int_{x_1}^{x_2}x^{(n+a)/(1-a)}(1-x)^{q/(1-q)}dx, \tag{4}$$

where $x_1=(1-q)\beta\varepsilon$, $x_2=x_1k_m^{1-a}\gg x_1$, and the normalization constant A is determined by the condition

$$A\int_{x_1}^{x_2}x^{a/(1-a)}(1-x)^{q/(1-q)}dx\equiv\langle k^0\rangle_q=1.$$

In the limit $a\rightarrow 1$, corresponding to a degenerate hierarchical tree for which only one node branches at each level, the expression $(1-a)^{-1}k^{1-a}$ in the distribution (3) becomes $(j-1)^{-1}\ln k$, where $j>1$ is the branching index. For a regular tree, each node of which undergoes a constant branching j, one has $N_k=j^k$, and the indicated expression is replaced by $-j^{-k}/\ln j$ (Ref. 5).

It is not difficult to see that in the continuum limit $1\ll k\ll k_m$ the finite-difference equation (3) can be put into the form of the condition $J_k=0$ for the generalized flux $J_k=F_kP_k-D_k(\partial P_k/\partial k)$, given by the effective force $F_k=-\varepsilon P_k^{q-1}\equiv -q^{-1}(\partial U/\partial P_k)$ and the diffusion coefficient $D_k\equiv N_k$. Hence it follows that expression (3) is a stationary solution of the Fokker–Planck equation $\partial P_k/\partial t+\partial J_k/\partial k=0$ (where t is the time) describing diffusion along the nodes of a hierarchical tree. In the self-similar regime, where the behavior of the system is determined by the time dependence $k_c(t)$ of the characteristic level of the hierarchy $1\ll k_c\ll k_m$, the distribution $P_k(t)$ is a homogeneous function $P_k(t)=k_c^\alpha(t)\pi(\kappa)$, where $\kappa\equiv k/k_c$.[4] The normalization condition gives the exponent $\alpha=-1$, and substitution into the Fokker–Planck equation gives $k_c^q\propto t$ and an integral equation for the function $\pi(\kappa)$ [for $q=1$ the latter, as expected, gives an exponential function for $\pi(\kappa)$].[6] Thus, as time passes, increasingly deeper hierarchical levels $k\sim t^{1/q}$, which are realized with probability $P_k(t)\propto t^{-1/q}$, become important in the behavior of the self-similar system.

The fact that the characteristic value of $k_c(t)$ increases monotonically with time makes it possible to use the hierarchical level number k as an effective time. The relation (2) appears not as the first integral of the Fokker–Planck equation but rather as the equation of motion for the renormalized probability $0<x_k<\infty$. To introduce the latter we shall examine a self-similar hierarchical system corresponding to a homogeneous hierarchical tree (we note that previously the condition of self-similarity was imposed on the state distribution in phase space, while here it characterizes an ultrametric space in which the hierarchically subordinated statistical ensembles are distributed). For such a system we can write[4] $P_k=\xi^k x_k \equiv j^{-k/D}x_k$, where the similarity parameter $\xi<1$ is determined by the fractal dimension $D=\ln j/\ln \xi^{-1}$, which in turn is related with the parameter q, used above, by the equation $q=1-D$ (Ref. 5). As a result, expression (2) assumes the form of the Landau–Khalatnikov equation

$$\frac{\partial x_k}{\partial k}=-\frac{\partial V}{\partial x_k}, \quad V(x)\equiv\frac{\varepsilon}{1+q}x^{1+q}-\frac{\ln j}{2(1-q)}x^2. \tag{5}$$

The effective potential $V(x)$ possesses a maximum at the point $x_c=[(1-q)\varepsilon/\ln j]^{1/(1-q)}$, which recedes to infinity as $q\rightarrow 1$. According to Eq. (5), to include the lower levels of the hierarchy the system must overcome a barrier of height $V_c=\varepsilon(1-\varepsilon/2)x_c^{1+q}/(1+q)$, after which x_k will grow without bound with increasing number k of the hierarchical level. We note that such a transition to a self-reproducing hierarchy regime is possible only for nonadditive systems $(q\neq 1)$, and the minimum barrier height corresponds to the case $q=0$, for which the coupling between the levels $U(P)=\varepsilon$ is maximum. In the limit $x_k \gg x_c$ the quadratic term makes the main contribution to the potential $V(x)$ and the solution of Eq. (5) assumes the simple form $x_k=P_\infty j^{k/(1-q)}$, where P_∞ is an integration constant. The initial probability $P_k\equiv j^{-k/D}x_k=P_\infty$ becomes independent of the level in the hierarchy. Although the calculations performed above pertain to a homogeneous hierarchical tree, there is hope that, qualitatively, the conclusion that the transition to a self-reproducing hierarchy is of an activational character will remain unchanged.

Stochastic effects are important before and after a hierarchical structure is formed. Their influence can be taken into account by adding to Eq. (5) white noise with intensity Θ that does not reduce to the temperature β^{-1}. These effects give rise to fluctuation activation above the barrier V_c, resulting in nucleation of a hierarchical structure in time $T=\tau\exp(V_c/\Theta)$, where τ is the relaxation scale. At the same time, after a time $t_m=T+\tau k_m^q$ has elapsed, these fluctuations integrate the ensembles corresponding to different nodes of the hierarchical tree. Assuming that the barriers separating these ensembles are determined by the expression Φk^{-D}, $\Phi>0$, and $D=1-q$, the formation time of a single ensemble at the kth hierarchical level is $\tau_k=\tau\exp\{(\Phi/\Theta)k^{-D}\}$. The total probability that a hierarchical system decays at time t is

$$\mathcal{P}_q(t)=\sum_k P_k^q e^{-t/\tau_k}.$$

Then, using the method of steepest descent, it is easy to see that the terms determined by the equation $t\exp\{-(\Phi/\Theta)k^{-D}\}\approx(q/D)(1-q)^{-1}(\Theta/\Phi)k^{1+D}$ make the maximum contribution to the sum indicated. At moderate times $\tau<t<t_m$, when the exponential reduces to 1, we obtain a solution of the self-similar type $k^{2-q}\propto t$, which corresponds to an exponential function $\mathcal{P}_q(t)$. In the limit $t\gg t_m$ we have $k^{-D}\approx(\Theta/\Phi)\ln t$, and the decay probability of a hierarchical system grows logarithmically with time

$$\mathcal{P}_q(t)\propto\left[1-\frac{1-q}{1-a}\left(\frac{\Phi}{\Theta}\right)^{(1-a)/(1-q)}\varepsilon\left(\ln\frac{t}{\tau}\right)^{-(1-a)/(1-q)}\right]^{q/(1-q)}. \tag{6}$$

This is the stage that corresponds to the formation of a single thermodynamic ensemble characterized by the Gibbs distribution.

This work was supported by the Ukrainian Ministry of Science (Grant No. 2.4/4).

*e-mail: Alexander@olem.sumy.ua

---

[1] C. Tsallis, Physica A **221**, 227 (1995).
[2] T. C. Helsey, M. H. Jense, L. P. Kadanoff *et al.*, Phys. Rev. A **33**, 1141 (1986).
[3] P. A. Alemany, Phys. Lett. A **235**, 452 (1997).
[4] A. I. Olemskoi, in *Physics Reviews*, Vol. 18, Part 1, edited by I. M. Khalatnikov, Gordon and Breach, London, 1996.
[5] A. I. Olemskoi and A. D. Kiselev, Phys. Lett. A **247**, 221 (1998).
[6] A. I. Olemskoĭ, Usp. Fiz. Nauk **168**, 287 (1998).

Translated by M. E. Alferieff